General Disclaimer

One or more of the Following Statements may affect this Document

- This document has been reproduced from the best copy furnished by the organizational source. It is being released in the interest of making available as much information as possible.

- This document may contain data, which exceeds the sheet parameters. It was furnished in this condition by the organizational source and is the best copy available.

- This document may contain tone-on-tone or color graphs, charts and/or pictures, which have been reproduced in black and white.

- This document is paginated as submitted by the original source.

- Portions of this document are not fully legible due to the historical nature of some of the material. However, it is the best reproduction available from the original submission.

NASA CR-
WRL 2122-14-F

FURTHER INFRARED SYSTEMS STUDIES FOR THE EARTH RESOURCES PROGRAM

by

J. Braithwaite, L. Larsen, and E. Work

INFRARED AND OPTICS LABORATORY
WILLOW RUN LABORATORIES
INSTITUTE OF SCIENCE AND TECHNOLOGY
THE UNIVERSITY OF MICHIGAN

prepared for

NATIONAL AERONAUTICS AND SPACE ADMINISTRATION

NASA Manned Spacecraft Center
Contract NAS 9-8381
W. E. Hensley, TF4, Project Manager

NOTICES

Sponsorship. The work reported herein was conducted by the Willow Run Laboratories of the Institute of Science and Technology for the National Aeronautics and Space Administration under NASA Contract NAS 9-8381 with Mr. W. E. Hensley/TF4, Earth Resources Office, as Project Manager. Contracts and grants to The University of Michigan for the support of sponsored research are administered through the Office of the Vice-President for Research.

NASA CR-
WRL 2122-14-F

FINAL REPORT

FURTHER INFRARED SYSTEMS STUDIES FOR THE EARTH RESOURCES PROGRAM

by

J. Braithwaite, L. Larsen, and E. Work

INFRARED AND OPTICS LABORATORY
WILLOW RUN LABORATORIES
INSTITUTE OF SCIENCE AND TECHNOLOGY
THE UNIVERSITY OF MICHIGAN

prepared for

NATIONAL AERONAUTICS AND SPACE ADMINISTRATION

December 1969

CONTRACT NAS 9-8381

NASA Manned Spacecraft Center
Houston, Texas 77058
W. E. Hensley/TF4, Project Manager
Earth Resources Office

FOREWORD

The work described in this report was conducted by the Infrared and Optics Laboratory (M. R. Holter, Head) of Willow Run Laboratories, a unit of The University of Michigan's Institute of Science and Technology. D. Lowe was Principal Investigator. The work and the writing of this report were coordinated by J. Braithwaite. In addition, the following people were responsible for specific aspects of the work and the corresponding sections of the report:

L. Larsen—Preamplifiers, Telemetry, and Signal Handling
E. Work—Structures
S. Lampert—Telemetry
J. Cook—Ground Receiving Stations

The work reported is closely related to Willow Run Laboratories' comparative multispectral remote-sensing program, in which improvements are sought in the kinds and qualities of data obtainable and in the quality, speed, and economy of the image-interpretation process.

This research was performed for NASA's Manned Spacecraft Center under Contract NAS 9-8381 and is related to and, in many respects, dependent upon the work completed by Willow Run Laboratories for NASA's Manned Spacecraft Center under Contract NAS 9-7156, for the U. S. Geological Survey under Contracts 14-08-001-10053 and 14-08-001-10108, for NASA's Marshall Space Flight Center under Contract NAS 8-21000, and for the U. S. Department of Agriculture under Contract NsG 715. The Willow Run Laboratories' number for this report is 2122-14-F.

ABSTRACT

This report discusses the development of design concepts and specifications for multispectral scanners for use from orbit as part of the Earth Resources Program.

The performance of such scanners may be limited by component performance, by weight and power allocations, and by the data rates and bulks which can be returned to the ground. Some of the more critical of these factors have been examined in detail, and methods of dealing with them have been investigated. It is shown, for example, that a 7-channel scanner with a 200-ft ground resolution is feasible, but that the swath width would be limited to less than 20 miles unless telemetry bandwidths larger than those in current use are made available.

CONTENTS

FIGURES

TABLES

FURTHER INFRARED SYSTEMS STUDIES FOR THE EARTH RESOURCES PROGRAM

Final Report

SUMMARY

Consideration is given to the factors affecting selection of a multispectral scanner to be used in earth orbit for earth resources investigations. The spatial and spectral resolution requirements needed for earth resources investigations are becoming known as a result of the various airborne programs. However, sensitivity considerations involved in the much greater altitude of orbital flight require that both spectral and ground resolutions be less than those readily obtained from aircraft. The data rate which can be handled conveniently is another constraint affecting the design of the experiment. Direct telemetry to a ground station affords the best solution. With current S-band systems, it would be possible to transmit the data obtained in seven spectral bands, each having a bandwidth of about 35 kHz. This, in turn, would impose a trade-off between ground resolution and swath width. For instance, at 300-ft ground resolution, the swath width could be at most 45 nmi. A mechanically simple scanner employing a conical scan is recommended.

An AGC/ALC system would be needed to match the signals to the dynamic range of the telemetry link, and the various procedures which could be used have been explored.

Various methods of cooling thermal-band detectors have been reviewed. Several practical methods are available. The preferred one will only become apparent as the integration of the experiment with the spacecraft and flight plan proceeds.

In order to achieve the fine angular spatial resolution required, the thermal-band detectors will have to be cold shielded to obtain optimum performance. This cold shielding increases the detector resistance so that preamplifier design becomes an important consideration. Our study shows that adequate preamplifiers can be designed.

Some alternative scan mechanisms are discussed. A nodding mirror with most of each cycle spent on a linear one-way sweep appears preferable to the simple conical scan. The mechanical design of such a nodding scan mirror is problematic, although it is being attempted in the Earth Resources Technology Satellite Program.

1
INTRODUCTION

The work described in this report was carried out between 22 June 1968 and 31 July 1969 under a contract with NASA's Manned Spacecraft Center (MSC) in Houston, Texas. The Contract Work Statement included a series of tasks involving the use of infrared technology in manned orbital earth resources experiments. Other tasks required the provision of engineering support to MSC from time to time. At the request of the Technical Monitor, several of these engineering support tasks were undertaken. Since the results of these tasks have been reported elsewhere, they are only enumerated and very briefly described in this report (sec. 2).

As a result of the effort which had to be put into the engineering support tasks and as a result of the overall developing situation, the emphasis on the remaining tasks was revised in collaboration with the Technical Monitor about midway through the program. In particular, tasks relating to the engineering design of orbital scanners and spectrometers were omitted. The remaining tasks, then, concentrated upon the conceptual designs of optical-mechanical scanners for use in the Apollo Applications Earth Resources Program. The designs were to be optimized to make best use of available data-handling systems, because these have always proved to be a limiting factor in the development of orbital-scanner concepts. Since it was necessary to determine the data rates which could be handled on AAP missions, a significant part of our study involved existing data-handling and telemetry systems.

In the revised Work Statement, several of the tasks were divided into two phases, the first phase dealing with concepts which could be implemented at once, and the second with more advanced concepts for later implementation. While the division of efforts among the tasks has closely followed the contractual allocation of funds, somewhat more effort than originally intended has probably gone into the immediate implementation phase of each task.

The results of our research on orbital scanning systems are presented in section 3. Each subsection refers to a task or group of tasks designated in the Contract Work Statement, and the order of the subsections corresponds to that of the Work Statement. It will be appreciated that section 3.4, the Conceptual Design Study, depends on the results described in the other subsections, but otherwise, these are essentially independent studies. Supplementary material for the various subsections is presented in the appendixes.

2
ENGINEERING SUPPORT TASKS

The following engineering support tasks were carried out at the request of the Technical Monitor. The discussion here is restricted to a brief description of the nature of each task.

Texas Instruments RS14 Review

Two members of the laboratory staff participated in an MSC review of this scanner at the Texas Instruments plant in Dallas on October 9, 1968.

Scanner-Calibration Study

The designs and installations of the two airborne scanners in current use in the MSC Earth Resources Program—the Reconofax IX and the RS-7—were studied to determine the best means of converting these instruments to measure radiance in an absolute rather than in a qualitative manner through the introduction of calibration sources. The conclusions were given in an oral presentation at MSC and documented in a written report.

Bendix Multispectral Scanner and Ground Data System

Laboratory staff participated in a preliminary design review held at the Bendix Aerospace Systems Division Plant in Ann Arbor on March 20-21, 1969. A letter report containing various recommendations on this program was submitted to MSC shortly thereafter.

Aircraft Flights

Three flights by Infrared and Optics Laboratory's multispectral-scanner-carrying aircraft were requested. A successful flight was made over the Tippecanoe agricultural test site during July 1968 and another over the Tennessee Valley test site No. 177 during October 1968. A third flight, requested for test site 44, Purdue, Indiana, for mid-November, was postponed and finally abandoned because of unfavorable weather, although some charges accrued to the contract as a result of preparations for this flight.

3
ASPECTS OF ORBITING SCANNERS

3.1. CRYOGENIC TECHNIQUES FOR ORBITAL APPLICATIONS

Any of the methods used in aircraft, field, or laboratory applications for cooling infrared detectors could be adapted to orbital use. One of these methods, storage of a cryogenic material in solid form, was in fact developed with space applications in mind. In addition, cooling by optical coupling to a cold, space background, not feasible inside the earth's atmosphere, has been used in space. The preferred method for a specific application would depend on the operational requirements and limitations, such as the temperature to be achieved, the thermal load, the time over which the system must remain operational, the duty cycle required, and the weight and power allotments.

To the best of our knowledge, only two methods have been developed for extended use in space: radiative cooling by optical coupling to cold space and solid cryogenic storage. As a

result, in any early application in which development time or cost has to be minimal, one of these two methods would probably be preferred.

3.1.1. RADIATIVE COOLING

Radiative cooling has been employed to cool the PbSe detector in the NIMBUS high-resolution infrared scanner. Since neither a power source nor a thermal sink has to be provided by the spacecraft, this is a preferred system when feasible. It suffers from two important defects. First, the temperature which can be reached appears to be limited by practical considerations to about 100°K, and there appear to be differences of opinion as to the practicability of cooling (HgCd)Te detectors by these means. Also, radiative cooling of the doped Ge detectors doesn't appear practical, since these detectors require much lower temperatures than can be obtained by this method. Second, radiation from the major sources in near earth space, i.e., from the sun and the earth, must be prevented from entering the system. This means that both the location of the experiment on the spacecraft and the orientation of the spacecraft are critical, and it seems unlikely that this method would be practical on a manned multipurpose-experiment carrier. However, its advantages are so great that the possibility of its use should always be considered.

3.1.2. SOLID CRYOGENICS

The solid cryogenics technique was pioneered by Aerojet-General Corporation and developed by Aerojet and other companies. In particular, Goddard Space Flight Center procured from Lockheed Missiles and Space Company a space-qualified, two-stage model capable of maintaining a mercury-doped germanium detector at its operating temperature for several months in space. To the best of our knowledge such systems have not been operated in space. However, since they have no moving parts, there seems no reason to suppose that they would present a reliability problem. While they are somewhat cumbersome and require special charging equipment to be connected to the apparatus as late as possible in the launch count-down, such systems appear to be the preferred method for manned orbital earth resources flights at the present time.

3.1.3. THE JOULE-THOMSON, OPEN-CYCLE CRYOSTAT

The Joule-Thomson, open-cycle cryostat has proven very satisfactory for military operations in which extensive standby times and short operating times are required, and thus it might be appropriate for a planetary flyby but not for an extended earth-orbiting system, even for one with a relatively low duty cycle. Also, the high-pressure gas supply bottles would probably not be welcomed on a manned experiment carrier. In manned spacecraft, however, supplies of cryogenic fluids are usually taken along in supercritical state for use in the propulsion and life-support systems. The temperature of these fluids varies as the contents are dissipated, but it would appear to be practical to use an open-cycle, Joule-Thomson cryostat to obtain appropriate temperatures.

Thus, if, for example, an emergency reserve of fuel hydrogen were available at the time the scanner was to be used, this fuel could conveniently be used with a Joule-Thomson cryostat, since the cryostat and the necessary tubing and controls are quite small and light. However, the feasibility of this method has not been examined in detail, and development would be needed for a viable system. Also, as explained in the next subsection, nozzle blocking is still considered a problem with these cryostats.

3.1.4. CLOSED-CYCLE SYSTEMS

The early closed-cycle systems based on Joule-Thomson cryostats with remote compressors or on Stirling cycle engines were developed for airborne use. While the reliability of these systems has improved considerably with development, blocking of the expansion orifice of the former and the necessary maintenance functions for both lead most experts to believe that they are unsuitable for extended use in space. Use of the Gifford-McMahon cycle developed by A. D. Little gives a reliable and maintenance-free cooling engine, but a remote compressor is still required with attendant maintenance problems. The use of a Vuillemier cycle engine by Hughes [1] appears to circumvent these problems and is expected to become a preferred method for space use when the power required and which must be dissipated (from 1/2 to 1 kw in current practice) is not a problem.

3.2. DETECTOR-PREAMPLIFIER PERFORMANCE

Ultimately the performance of a scanner is determined by the signal-noise ratio (SNR) achieved by the detector when measured in the electronic bandpass of the overall amplification and recording system. In practice, the SNR is inevitably degraded in the electronics. Section 3.6 deals with methods of avoiding unnecessary SNR degradation which results when the amplified signal level lies outside the dynamic range of subsequent stages in the chain. In this section the problem of providing preamplifiers which do not appreciably degrade the SNR available at the detector is considered.

The general nature of the problem can be illustrated using figure 1. This figure shows in an idealized way how the signal and the important kinds of noise associated directly with the detector vary with frequency. In principle, the 1/f and generation-recombination (g-r) noise, which are proportional to bias current, can be increased by increasing the bias voltage. Thus, in principle, they can be made to predominate over Johnson noise; however, in practice, effects such as breakdown and Joule heating may prevent this. In fact, with some poor detectors the knee in the g-r noise at the frequency corresponding to the intrinsic time constant (τ_o) of the detector is not observed. It should be noticed that the ratio of signal to g-r noise is not affected by this knee, although at higher frequencies, Johnson noise, unaffected by this time constant, will eventually predominate and swamp the signal. In any case, it is desirable to design a preamplifier

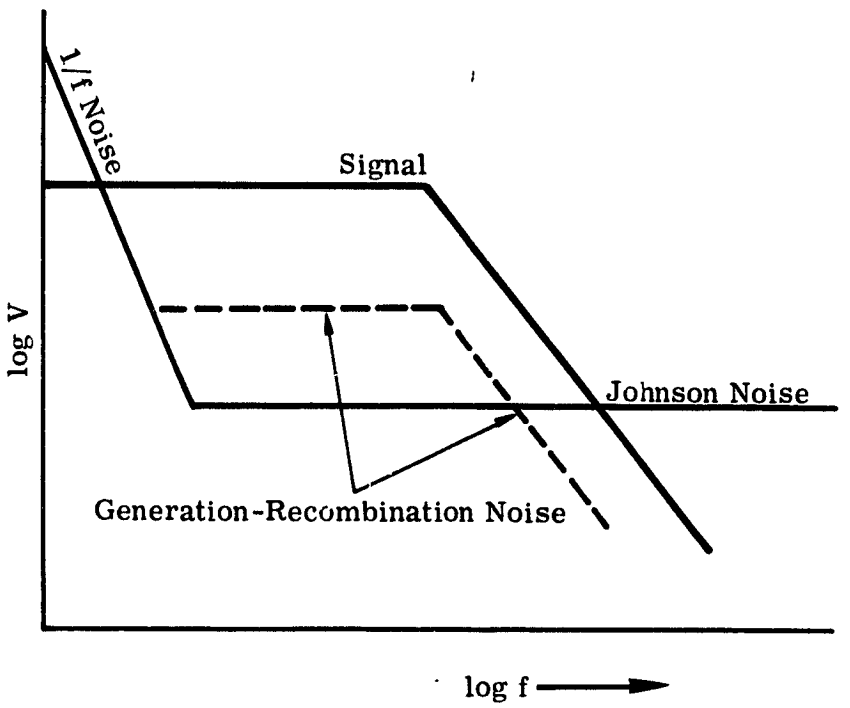

FIGURE 1. VARIATION OF SIGNAL AND NOISE WITH FREQUENCY (IDEALIZED CONCEPTION)

which contributes appreciably less noise than that associated with the detector. Such a task is generally straightforward when ambient photon fluxes are falling on the detector and when modest electronic bandwidths are involved. If, however, the photon flux is greatly reduced, the g-r noise is reduced, and the detector impedance is increased. Thus, while it is a straightforward matter to build preamplifiers for, say, Ge:Hg detectors facing a hemisphere of 300°K radiation, if the background flux is greatly reduced, the task becomes more difficult. That the background flux may be reduced by several orders of magnitude can be seen from the following example.

In a scanner it can be shown by simple geometry that the detector width, d, is given by

$$d = D\phi F$$

where D is the diameter of the collector

ϕ is the instantaneous field of view

F is the beam f/number at the detector.

0.2 mm is generally considered the minimum practical size for a Ge:Hg detector with a high D*. Then for D = 20 cm and $\phi = 10^{-4}$ rad, we find that

$$F = \frac{0.02}{20 \times 10^{-4}} = 10$$

To maximize the SNR, cold shields which emit a negligible number of photons must be provided to reduce the field of view to F/10. The number of photons received from F/10 compared to those from the complete hemisphere is

$$\frac{\pi}{4}\frac{(1)^2}{10} \times \frac{1}{\pi} = \frac{1}{400}$$

If, in addition, the wavelength passband is reduced to 1 μm near 10 μm by cold filtering, a further flux reduction of about 7.5 times is effected, giving a total reduction of 3000 times.

The number of papers appearing in Proc. IRIS [2-7] shows that a good deal of attention has been paid to this subject. Unfortunately, most of these deal with extreme reduction in background flux and/or relatively small electronic bandwidths. As a result of the papers' subject matter as well as some ambiguity in presentation, attempts to apply the material presented to the present problem proved unsatisfactory. However, a number of representatives of detector manufacturers were contacted during and following the National IRIS meeting (May 20-22, 1969). On the basis of these discussions and of further calculations carried out subsequently, there is little doubt that it will be possible to build preamplifiers, using conventional transistor technology, that will be adequate for service in the classes of scanners described in section 3.4. In general, it will be necessary to use low noise-level resistors and to mount these inside the cryostat at, or close to, detector temperature in order to achieve sufficiently low noise contributions.

An example calculation of the sort on which this conclusion rests is given in appendix I. However, further work should be done in this area, both with respect to detectors for the 8-14-μm band and with respect to semiconductor detectors for use at shorter wavelengths.

3.3. MECHANICS OF SCANNING STRUCTURE

The use of optical-mechanical line scanners is not new in reconnaissance and remote sensing. In the several decades that such scanners have been in use, many unique and sometimes complex scanning techniques have been introduced. The scan mirrors associated with object plane scanners, however complex, may be classified into one of three general categories: (1) the single-faced scanning mirror, (2) the multifaced scanning mirror, and (3) the rotating, multifaced, reflecting prism. Examples are shown in figure 2.

Common to any of these three classifications is the need for an optically flat reflecting surface or surfaces. The degree of spatial resolution desired determines the necessary degree or quality of optical flatness. Improved performance, as spurred on primarily by the military, has implied better spatial resolution and greater imagery contrasts, necessary to facilitate recognition by pattern or shape. Most of the newer military scanners are of the multifaced scan mirror type or the rotating-prism type.

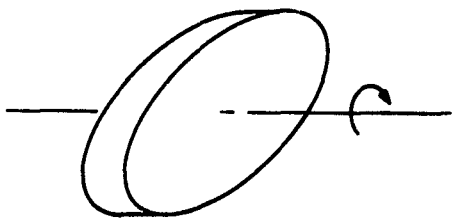

(a) Single-Faced Scanning Mirror

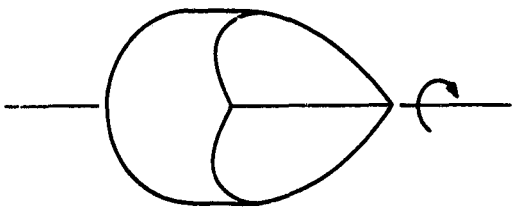

(b) Multifaced Scanning Mirror

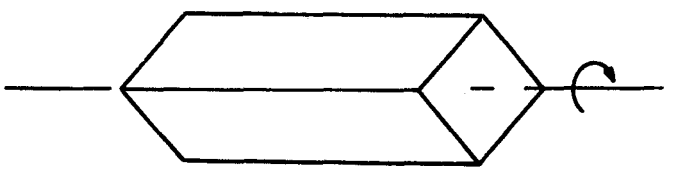

(c) Multifaced Reflecting Prism

FIGURE 2. TYPES OF SCANNING MIRRORS

A number of analytical and experimental studies have been made regarding scan mirror deformation of some of the higher performance military scanners [8, 9, 10].

Recent trends in the field of environmental sensing, while not subordinating the importance of spatial resolution and contrast, have put great emphasis on target differentiation by spectral characteristics and on the need for quantitative data. The acquisition of multispectral data is primarily a detector problem. However, the added burden of quantitizing this multispectral data

requires consideration of the complete scanner optical system. The requirement for quantitative data dictates that varying radiation from unknown sources will not be received at the detector (or spectrometer entrance slit). The multifaced scan mirror and rotating prisms inherently do not meet this criterion. The uncertainty introduced by the multiple faces of a scan mirror or prism is particularly difficult to deal with in the thermal infrared region. Furthermore, a quantitative scanner is more accurate if a fixed optical path within the scanner is utilized throughout the entire scan as well as during the introduction of calibration sources. Again, such is not the case with a multifaced scanner and particularly not with the rotating-prism scanner, in which different pairs of folding flats are used to share the function of relay mirrors in varying proportions, depending on the position of the scan mirror at any one instant.

These considerations have led to a renewed evaluation of the performance which can be expected from a single-faced, rotating scanning mirror of the type illustrated in figure 3. In its elementary form it is a flat plate centrally secured to a shaft—the assembly mounted in a cantilevered or overhung manner. The reflecting surface is oblique to the axis of the shaft, with the degree of obliquity somewhere between the nearly normal condition and 45^{o} away from the normal. In reality such a scan mirror would have a somewhat different mass distribution for purposes of balancing and improved rigidity. However, for the purposes of this paper we will assume a monolithic system such as is shown in figure 3.

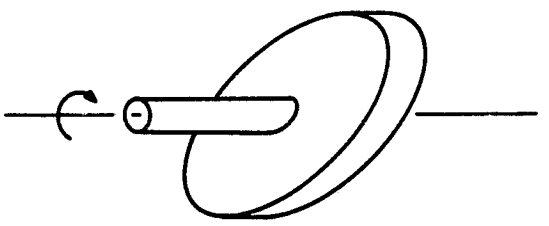

FIGURE 3. SHAFT-SUPPORTED, OBLIQUELY MOUNTED, SINGLE-FACED, ROTATING SCANNING MIRROR

In the remainder of this section we will consider the forces which deform the reflecting surface from its optically flat state as a result of the mirror's rotation. An equation for the bending of a circular plate under a linearly varying load will be utilized to describe quantitatively the deformation of such a scan mirror.

Figure 4 shows a geometrical representation of an obliquely mounted elliptical plate. In the coordinate system chosen, the X and Y axes are in the neutral or middle plane of the plate, and they are coincident with the major and minor axes respectively of the ellipse. The Z axis

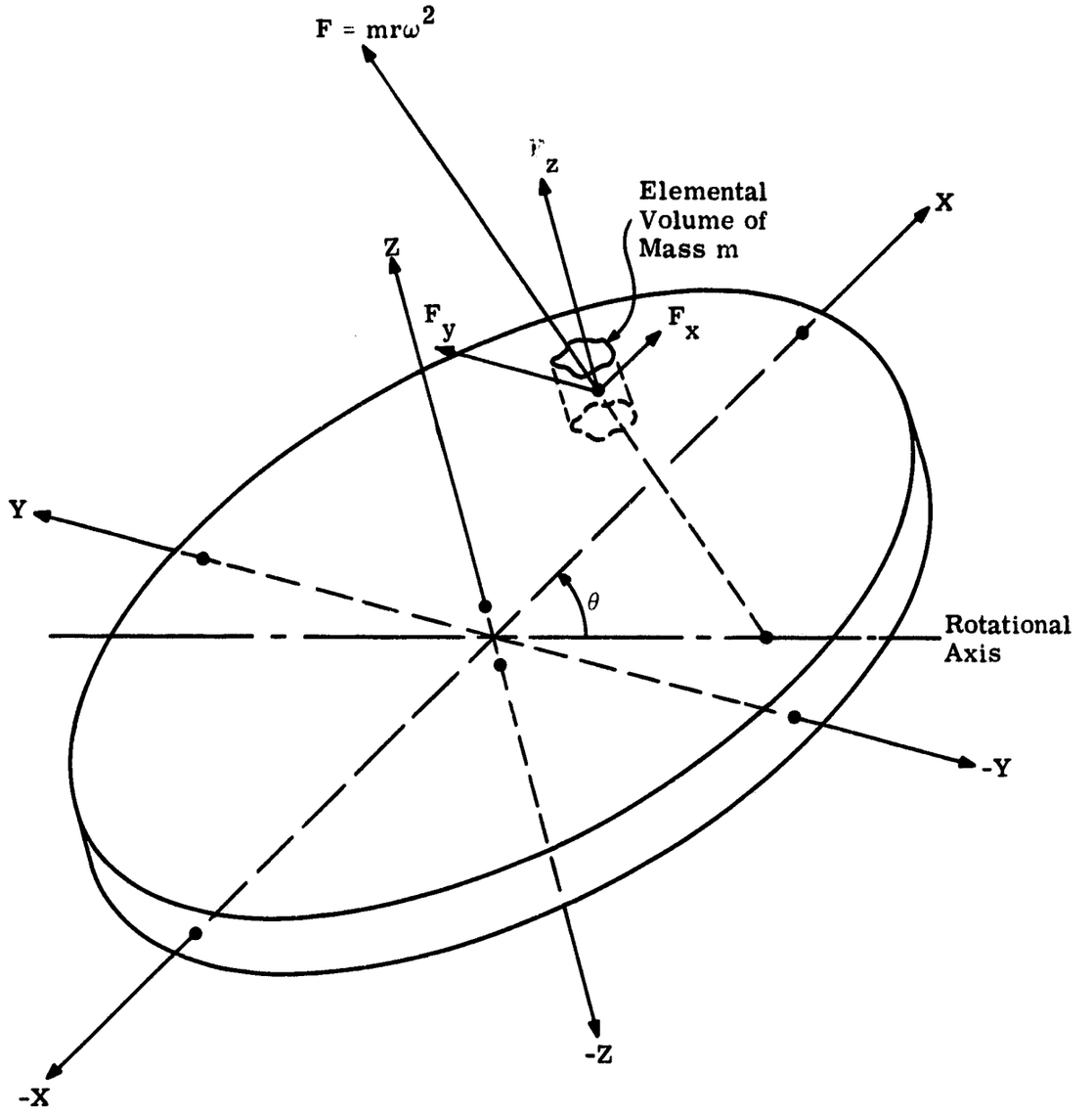

FIGURE 4. LOADING ON AN ELEMENTAL VOLUME OF AN OBLIQUELY MOUNTED, SINGLE-FACED SCANNING MIRROR

is normal to the neutral plane of the plate. The angle θ denotes the obliquity of the plate with respect to the rotational axis. The rotational axis passes through the origin and is coplanar with the X and Z axes.

If we ignore gravity, the loading to which the plate is subjected is entirely the result of centrifugal forces in the plate. The vector F in figure 4 represents the centrifugal force acting on a small elemental volume of the plate. Its line of action radiates from the rotational axis, passes through the centroid of this element, and lies in the plane normal to the rotational axis.

The force F may be resolved into its three orthogonal components F_x, F_y, and F_z, with F_x and F_y in the neutral plane of the mirror. The normal component F_z will then be assumed to be the only force influencing plate deflection. This is not perfectly true because if a slight bending of the plate should occur, the tensile forces F_x and F_y would tend to remove the bending. To neglect these forces will be to err only very slightly toward the conservative side.

Figure 5a shows the normal loading on the plate. Because this normal loading varies along the X axis directly as r (polar radius vector) varies, the loading can be described by a linearly varying envelope as shown in the figure. By simple geometry it can be shown that for any value of X, the normal force along the Y coordinate is constant. A normal view of the plate is shown

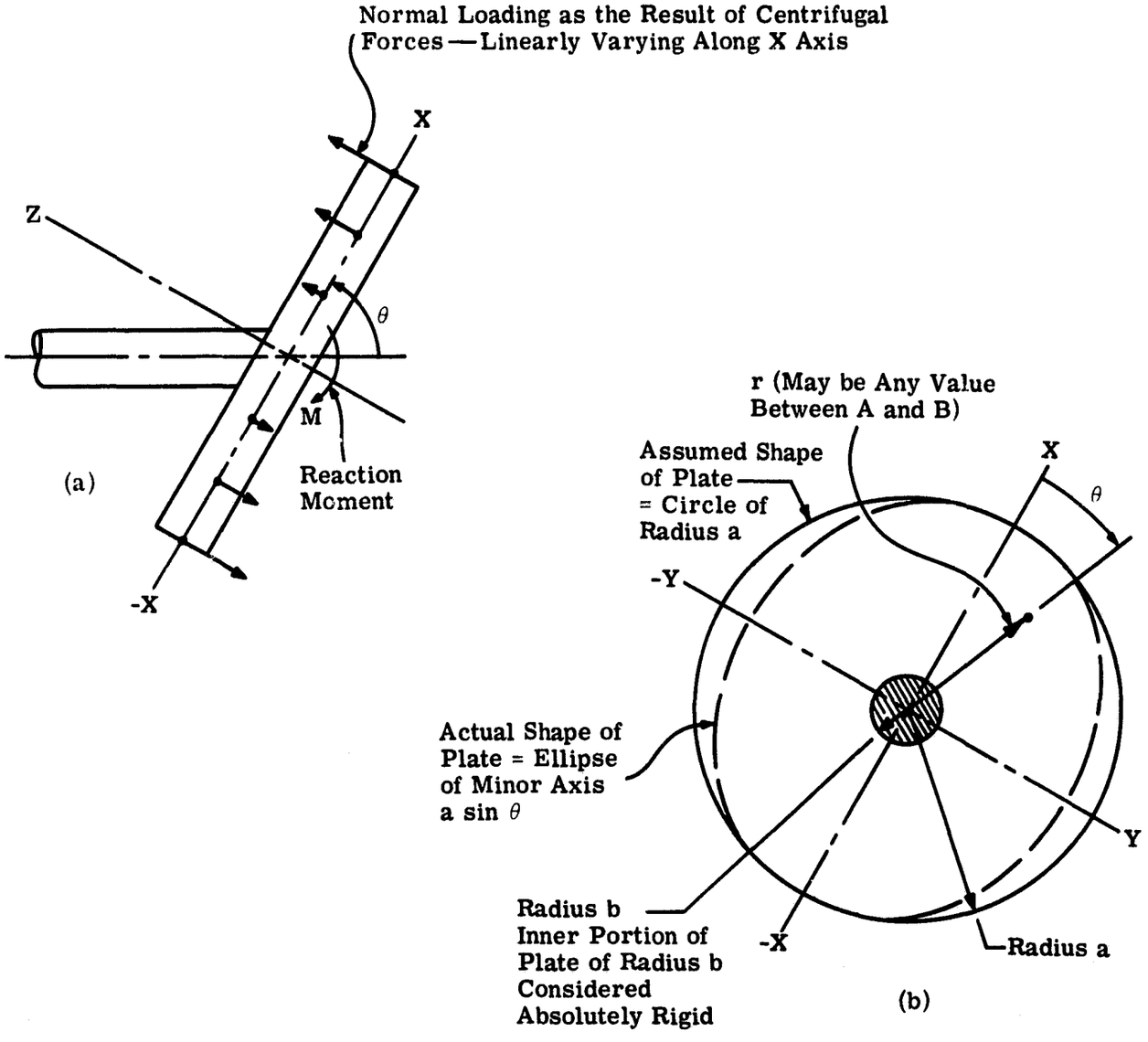

FIGURE 5. LOADING OF SCANNING MIRROR. (a) Normal loading on plate and (b) normal view of the plate.

in figure 5b. The inner portion of the plate, shaded in the figure and described by the radius b, is the attachment point for the shaft and is considered absolutely rigid. Note that we are considering the mirror, as viewed normally, to be circular, whereas it is, in fact, elliptical. For the approximation of bending herein being derived, this variance should not be significant.

A similar loading situation occurring quite regularly in construction practice has been investigated by Timoshenko and Woinowsky-Krieger [11]. Such a condition is encountered in the case of a circular foundation slab supporting a chimney. A moment M as the result of wind pressure on the chimney is transmitted to the slab. Timoshenko and Woinowsky-Krieger have assumed the reactions to this moment to be linearly distributed, resulting in the same kind of loading described above. The equation for the deflection of the chimney slab is as follows:

$$W = \frac{pa^4}{192D_f}(\rho + A\rho + B\rho^3 + C\rho^{-1} + D\rho \log \rho) \cos \theta$$

where

W = deflection of the plate in the direction of the Z axis

p = pressure load at outside edge (at $\theta = 0^o$)

θ = vectorial angle measured from X axis

D_f = flexural rigidity = $\frac{Eh^3}{12(1 - \upsilon^2)}$

E = modulus of elasticity

h = plate thickness

υ = Poisson's ratio

ρ = dimensionless ratio = r/a

r = polar radius vector which may vary between b and a

a = outside radius of circular disk

b = inner radius defining boundaries of portion of plate which remains absolutely rigid

A, B, C, and D = constants of integration defined by boundary conditions

The constant of integration A represents the rotation of the plate as a rigid body with respect to the diameter perpendicular to the loading diagram of figure 5a (the Y axis). Essentially it is the rotation of the mirror as a rigid body with respect to its support shaft. Therefore, since we are here only concerned with the induced bending or curvature occurring within the mirror and not with the rotation of the mirror as a whole, the term $A\rho$ can be eliminated from the previous equation. The other constants of integration for this particular case are:

$$B = -2\frac{4(2 + \upsilon) + (1 - \upsilon)\beta^2(3 + \beta^4)}{(3 + \upsilon) + (1 - \upsilon)\beta^4}$$

$$C = -2\frac{(2+\upsilon)\beta^4 - (3+\upsilon)\beta^2(3+\beta^4)}{(3+\upsilon)+(1-\upsilon)\beta^4}$$

$$D = 12$$

where β = dimensionless ratio b/a.

As an example, we will assume that a mirror of beryllium plate, 1.00-in. thick, obliquely mounted at 45°, is to be spun at 6000 rpm. The mirror is just large enough to fill a 9.00-in.-diameter aperture. The supporting shaft is 1.50 in. in diameter. Pertinent physical properties for beryllium are:

$$\text{Density: } d = \frac{0.066 \text{ lb}}{\text{in.}^3}$$

$$\text{Modulus of Elasticity: } E = 44(10)^6 \text{ psi}$$

$$\text{Poisson's Ratio: } \upsilon = 0.08$$

The pressure loading, p, occurring on the X axis, at the tip of the plate, and in a direction normal to the plate surface as a result of centrifugal loading is:

$$p = \sin 45^\circ(mr\omega^2)$$

$$= \sin 45^\circ\left(\frac{dh}{g}r\omega^2\right)$$

$$= (0.707\frac{(0.066)(1)}{(32.2)(12)}(4.50)(200\pi)^2$$

$$= 215 \text{ psi}$$

where ω = rotational rate of the mirror shaft

g = acceleration due to gravity

Other constants are:

$$D_f = 3.69(10)^6 \text{ in.-lb}$$

$$a = \frac{4.5}{\sin 45^\circ} = 6.36 \text{ in.}$$

$$b = \frac{0.75}{\sin 45^\circ} = 1.06 \text{ in.}$$

$$B = -5.46$$

$$C = 0.163$$

from which

$$W = 0.0021 \text{ in. at } \theta = 0^\circ \text{ and } r = a$$

As noted, this represents the tip deflection of the mirror. From the previous equation, a plot of the deflection occurring across the entire optical surface can be obtained. Figure 6 shows in greatly accentuated form the deflection occurring along the X axis (the major axis of the ellipse). Figure 7 is a contour plot of the magnitude of deformation occurring across 1/2 of the elliptically shaped flat. The contour plot graphically depicts the bending or curvature gradients in the optical surface. In fact, these gradients and the resultant angular spreading of the optical beam are our prime concerns. Figure 8 shows the loss in efficiency caused solely by the induced deformation of this mirror from its initial optically flat condition.

The result of this strain analysis has been (1) the application of a derived equation to one specific scan-mirror condition, and (2) a presentation of the results of the centrifugally induced deformations. However, it should be quickly pointed out that a usable scan mirror would, in fact, depart quite radically from the simple plate herein considered. For example, quite probably one would want to optimize the distribution of mass within the plate by utilizing a honeycomb or similar structure. Furthermore, one would probably want to add stiffening gussets in order to reinforce certain parts of the mirror, such as the extended mirror tip. Such a complicated structure quickly becomes exceedingly difficult to model and analyze, and an experimental study would perhaps better serve this end.

3.4. CONCEPTUAL DESIGN STUDY

3.4.1. THE RESOLUTION-SWATH WIDTH TRADE-OFF

Experience gained in preliminary planning of experiments for the AAP/B and AAP/1A concepts suggested that the most critical restriction on the conception and design of an optical infrared scanner experiment for manned orbital missions lies in the limits on data rate and bulk compatible with the overall mission concept and spacecraft system. When components and systems which will be readily available during the early 1970's are employed, the highest data rates are obtained by using line-of-sight S-band telemetry. While the coverage provided by the existing ground receiving stations is not worldwide, the U. S. A. is well covered, as shown in appendix VII, as are many other areas of interest. If a tape recorder with appropriate bandwidth could be found that would be suitable for the mission, it could be carried onboard and used to record data from any area overflown. The data could then be played back and telemetered to a ground station to give essentially worldwide coverage, limited only by orbital characteristics. Section 3.5 deals with the data rates that are in fact compatible with current S-band orbit-to-ground telemetry (TM) links. The answer depends on many factors, such as transmitter power, receiver-dish size, and coverage. Assuming reasonable values, such as 20 W of transmitter power, 30-ft receiver dishes, and 1/2% accuracy, it appears that seven channels, each with about 35 kHz of analog bandwidth, are possible. Although many alternative selections could be made, most of

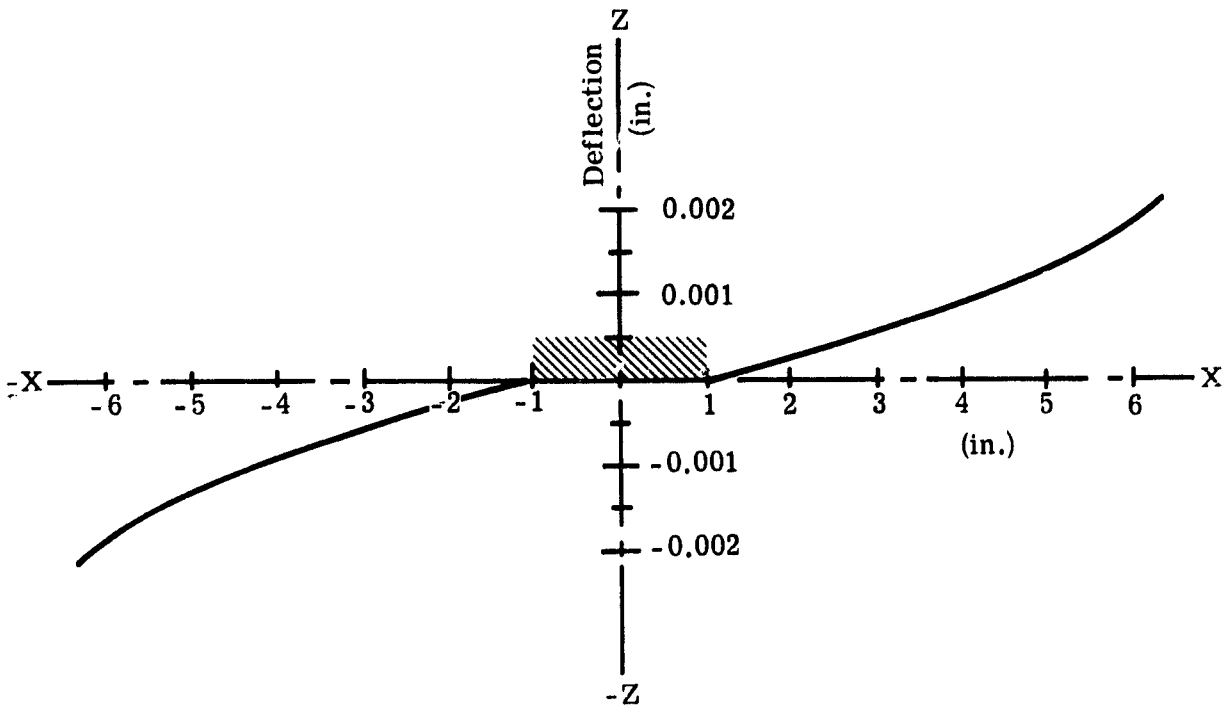

FIGURE 6. PLOT OF DEFLECTION OF MIRROR SURFACE ALONG THE X AXIS

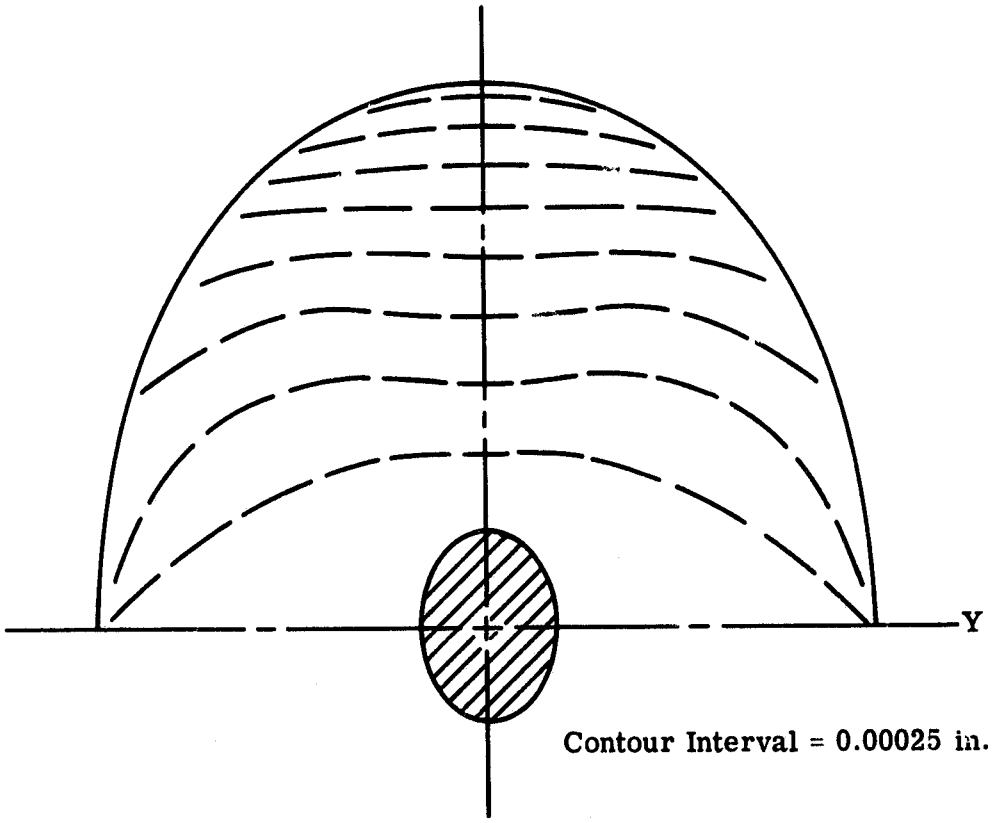

FIGURE 7. THE DEFORMED OPTICAL SURFACE INDICATED BY DEFLECTION CONTOURS

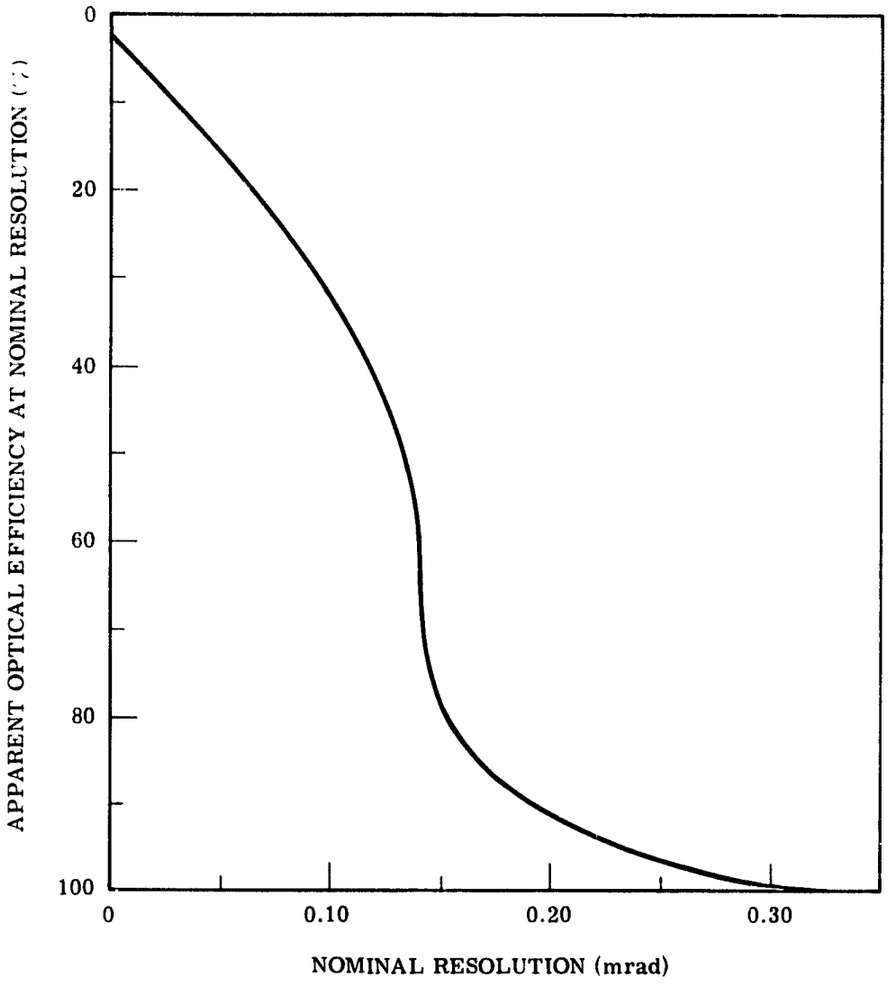

FIGURE 8. LOSS IN EFFICIENCY AS THE RESULT OF INDUCED DEFORMATION IN THE SCANNING MIRROR

the remainder of this section will be based on this particular selection. Corresponding results for alternate selections can be derived readily.

On this basis each channel can scan up to 70,000 ground resolution elements every second. In practice, this number might be reduced if the transmission duty cycle is less than unity* or

*NOTE: Suppose the scanner output has a bandwidth of Δf Hz, but only a fraction 1/a of each cycle is used. If the useful signal is perfectly reformated to use the narrowest possible transmitter bandwidth, then this will be the mean bandwidth: $\Delta f/a$ Hz (the bandwidth is zero during the remainder of the scan cycle). In practice it will not generally be possible to reformate perfectly, so the transmitter bandwidth will have to be at least slightly greater than $\Delta f/a$ Hz. The important thing to notice is that the instantaneous bandwidth is the one that must be used in calculating the system sensitivity but that the reformated bandwidth, which may be appreciably smaller, is the one which determines the transmitter specifications.

if a bandwidth less than half the reciprocal of the dwell time is used. For orbits likely to be used, the ground velocity is close to 24,000 ft/sec. For complete coverage with no overlap and for a ground resolution of a × a ft^2 over a swath width of b ft, the number of elements scanned per second is

$$\frac{24{,}000\ b}{a^2}$$

This can be equated to 70,000, the channel rate under consideration, to give a relationship between a and b. In practice, the swath width will be less because of the impracticability of perfect reformating, so if the transmitter bandwidth and a are fixed, then b must be somewhat less than that given by this relation. The relationship between a and b and a number of other related parameters is given in table I. (It is interesting to compare the specifications proposed for Goddard Space Flight Center's earth resources technology satellite (ERTS): six channels with ground resolution of 200 ft and a 100-mile swath width. Thus, ERTS requires appreciably more TM bandwidth than that considered in this section.)

TABLE I. RELATION BETWEEN RESOLUTION AND SWATH WIDTH

a Ground Resolution (ft)	m Elements Per Line	b Maximum Swath Width** (nmi)	β Angular Resolution (mrad)	ϕ Maximum Swath Width	ℓ Scan Lines/sec	rpm (For Single Detector and Scan Mirror*)
100	300	5	0.067	1.2°	240	14,400
150	450	11	0.10	2.6°	160	9600
200	600	20	0.133	4.6°	120	7200
300	900	45	0.20	10.5°	80	4800
400	1200	80	0.267	19.2°	60	
500	1500	125	0.33	28°	48	2880
700	2100	235	0.463	54°	34.3	2060
1000	3000	500	0.67	120°	24	1400

*If n detectors are used in each channel, the rpm should be multiplied by 1/n.

**For 250-nmi orbit.

We now proceed to investigate the sensitivity of the systems described in table I. This can be done in a general way by making assumptions about the various efficiencies involved in the calculation. We also assume that the optical bandwidths of the shorter wavelength channels are made wide enough so that the 10.5- to 12.5-μm thermal channel will have limiting sensitivity. This assumption is valid for the band selection used in the ERTS program, in which, however, the elimination of angular resolution or larger angular resolution in the thermal channel is accepted to simplify the hardware design. This band selection is as good as can be made at the present time and will be followed here. However, to study the relationship between the thermal and shorter wavelength bands, it seems best to divide the available TM bandwidth equally between the seven channels.

The signal power (Φ) falling on the detector is the product of the differential radiance of the target and its background ($\Delta L_\lambda \Delta\lambda$), the throughput of the scanner, and the optical efficiency of the latter. Thus:

$$\Phi = \Delta L_\lambda \Delta\lambda \frac{\pi}{4} D^2 \beta^2 \text{ (optical efficiency)}$$

where D = diameter of entrance aperture

β = angular resolution

Now the noise-equivalent power (NEP) of the detector is given by

$$\text{NEP} = \frac{\sqrt{\text{area} \times \Delta f}}{D^* \text{(electronic efficiency)}}$$

By simple geometry, the root of the detector area is given by $D\beta F$, where F = f/number at the detector. For Δf we can take the channel bandwidth, established earlier, divided by the scan efficiency. Anticipating selection of a scan method, we use a scan efficiency of 0.3, giving a value of Δf = 120,000 Hz. Electronic efficiency includes waveshape and noise factors, and we use a reasonable figure of 0.5. Thus

$$\text{NEP} = \frac{D\beta\sqrt{120{,}000}}{0.5} \times \frac{F}{D^*}$$

D^* at these wavelengths for cooled detectors is approximately 2×10^{10}. It would be possible to improve this by cold filtering to the 10.5- to 12.5-μm band to give a D^* of about 3×10^{10}, provided it would be possible to build an efficient preamplifier which matches the increased detector impedance. With the same restriction, it would be possible to employ cold shielding to enable use of a larger detector than that resulting from use of a low value of F to optimize the NEP. We could then make F = 1 and use the D^* corresponding to this F number. As shown in section 3.2, it is feasible to design preamplifiers for those bandwidths which remain efficient when the photon flux onto the detector is reduced to 1/1000 of the room temperature (T) background value, so provided that we do not make $F \gtrsim 10$, we can write:

$$\text{NEP} \cong \frac{760 D\beta}{3 \times 10^{10}}$$

Now looking for a system $\text{NE}\Delta T = 1/2^\circ C$, we can compute the $\Delta L_\lambda \Delta\lambda$ for the 10.5- to 12.5-μm band by using a radiation slide rule. We find that for $\Delta T = 0.5^\circ K$ and $T = 300^\circ K$

$$\Delta L_\lambda \Delta\lambda \cong 10^{-5} W \times cm^{-2}\text{-}sr^{-1}$$

Now

$$\text{SNR} = \frac{\Phi}{\text{NEP}} = \frac{10^{-5}(\pi/4) D^2 \beta^2 \text{(optical efficiency)}}{2.5 \times 10^{-8} D\beta}$$

Putting the optical efficiency equal to 0.3 we get

$$SNR = 100D\beta$$

Or to give a SNR of 1, we see that the collector diameter needed is given by

$$D = \frac{1}{100\beta}$$

If n adjacent detectors are used in each channel such that n adjacent scan lines are scanned simultaneously, then the scan rate can be reduced by 1/n times without losing coverage. This does not change the overall data rate, so the bandwidth required by the TM system is unaffected. However, the bandwidth in each detector-amplifier channel can be reduced by 1/n, and the NEP is thereby decreased by $1/\sqrt{n}$. Making this adjustment, the last equation becomes

$$D = \frac{1}{100\beta\sqrt{n}}$$

Some values of D derived from this equation for various values of β and n are given in table II.

TABLE II. RELATION BETWEEN APERTURE SIZE AND ANGULAR RESOLUTION

β (rad)	D (n = 1) (cm)	D (n = 3) (cm)
10^{-4}	100	58
$1\ 33 \times 10^{-4}$	76	44
2×10^{-4}	50	29
3.3×10^{-4}	30	17.5
6.7×10^{-4}	15	9

Since the detector size, d, is given by $D\beta F$, if we take, as explained in table II, $D\beta = 1/100$, we get for the detector size

$$d = F/100$$

If Ge:Hg detectors are used, then the smallest satisfactory size is about 0.025 cm, so we must make F = 2.5. This requires a degree of cold shielding which is quite practical, but if several detectors are used to make possible a reduction in D, then either the required d is reduced by $1/\sqrt{n}$ or else F must be increased by $\sqrt{n}$.

The two tables form a basis for selection of the specifications for an orbital scanner. A good deal of thought has been given to this problem, and a number of discussions were held with members of the Infrared and Optics Laboratory most closely in touch with Earth Resources Applications, as opposed to sensor design. Generally, fine ground resolution is required as well as the wide area coverage possible from orbital altitude. A 200-ft ground resolution is about the poorest which could be used to resolve agricultural fields, although with that resolution inhomogeneities in fields would rarely be resolved. From 250 nmi (1.5 million ft), 200 ft represents an angular resolution of 1.33×10^{-4} rad. It should be possible to obtain acceptable performance at this resolution with 3 detectors, an 18-in. optical system, and a swath width somewhat less than 20 nmi. Further consideration has shown that a relatively straightforward scanner can be designed to these specifications (a concept which will be discussed in more detail in a later subsection). The relatively narrow swath width would present a serious shortcoming to any investigator concerned with the coverage of specific test sites. Since only about 1/50 of the area of the U. S. would be covered in daylight each day, an investigator might have to wait months before his site was overflown in clear weather. The position would be improved if the experiment carrier could be rolled to aim the experiment at targets somewhat removed from the ground track. Even better, though probably more difficult to implement, would be use of a spacecraft the orbit of which could be changed as required. For example, a sun-synchronous, near-polar orbit could be made to pass over any point on the earth's surface at some time during a week by inducing a heading change of less than 1^{o} at an appropriate time.

Since some disciplines, such as aspects of oceanography and geomorphology, are interested in wide coverage at the expense of fine resolution, this requirement must also be considered. An angular resolution of 2/3 mrad can be obtained with a 6-in. aperture and gives close to horizon-to-horizon coverage. Previous studies have shown that these specifications can be implemented by use of a conventional 45^{o} mirror scanner of the HRIR type. Such a scanner would be quite straightforward in design and technology, so no further consideration is given to such a concept here. Although there is a case for orbiting such a scanner to investigate the value of wide area low-resolution coverage, the requirements of most earth resources investigators make it clear that such an experiment has low priority compared to the 200-ft ground-resolution scanners.

A compromise over the resolution-swath width trade-off would be possible if the signals from a high-resolution, wide-swath scanner could be tape-recorded over some region of interest and telemetered at a reduced rate so that the TM bandwidth is not exceeded. However, since the development of very sophisticated equipment would be required, such methods do not seem practicable for early AAP flights.

Perhaps a simpler method of trading coverage along the track for coverage across the track would be to use a form of image motion compensation, as shown in the diagram of figure 9. For instance, a square 100 nmi on each side and a 500×20-nmi strip contain the same number of

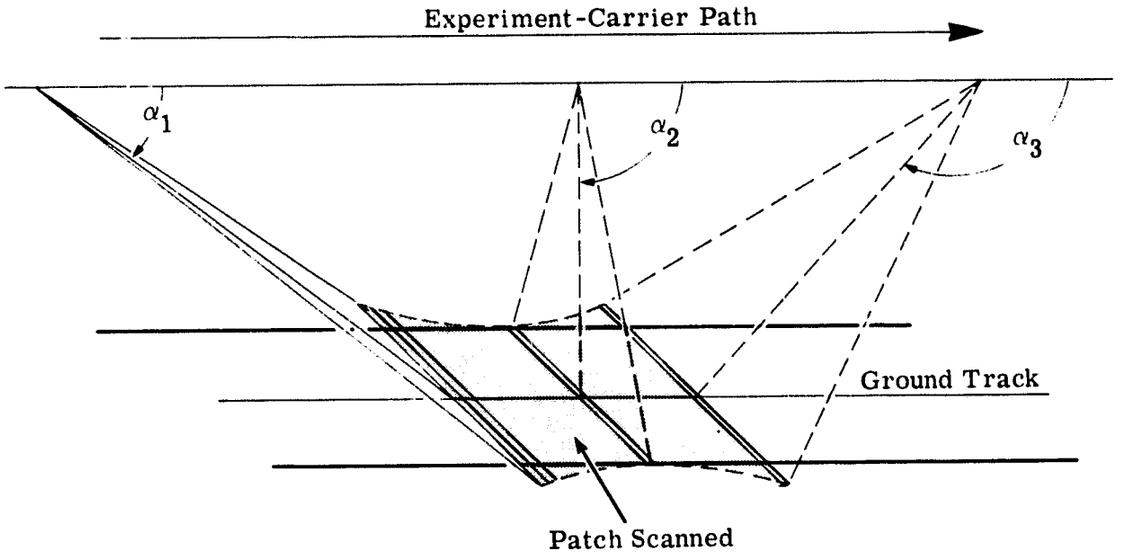

FIGURE 9. SCAN GEOMETRY FOR IMC SCANNER. $\alpha_1, \alpha_2, \alpha_3$ changing elevation of scan.

elements. Either could be scanned from a 500-nmi segment of a 250-nmi-high orbit by using an IMC scanner for the square or a regular scanner with the same data rate for the strip. The IMC scan leads to some difficulties of interpretation, because the view angle changes in two planes,* but otherwise, since the region scanned can be positioned at will on the ground track (provided TM coverage or an onboard recorder is available), a reasonable match for most user's needs is provided. The geometry of this scan is dealt with in appendix II. However, such a system would call for a good deal of sophisticated equipment and would require a high degree of spacecraft stabilization, so it is not considered practicable for an early AAP opportunity.

3.4.2. IMPLEMENTATION OF THE 200-FT GROUND-RESOLUTION SCANNER

Some Alternatives

A good deal of thought has been given to finding the best scan mechanism with which to implement a scanner giving a 200-ft ground resolution over a swath width of somewhat less than 20 nmi. From a 250-nmi orbit, this requires an angular resolution of 0.133 mrad over a total field of not more than 4.6°. Because of the small total field, a conventional 45° mirror scanner would have a very poor duty cycle and thus poor sensitivity for a given aperture size. In principle, a multifaced scan mirror could be used to increase the scan efficiency, but either a multifaced prism or a multifaced pyramid would be too large to be practical. As a result, one is led

*The variation of view angle is similar in nature to that occurring in a framing camera, except that in the direction of the track the IMC scanner looks IN at the corners rather than OUT at the corners.

to consider an object plane scanner with an oscillating scan mirror or one of the many other forms of image plane scanners. The scanners being studied by Hughes [12] and by Hycon [13] for the ERTS program are examples of these two approaches. Since we are considering a total field 5 times less than that considered for the ERTS, a reduced field version of the Hughes scanner would present a lesser engineering problem than the present ERTS version. On the other hand, for the Hycon approach, the reduced field implies the need for 5 times as many rotating-lens systems, so this approach seems impracticable. In addition, it would be necessary to replace the several refractive relay optics of this system with reflective systems in order to obtain the wide wavelength coverage needed, and this replacement would compound the problem.

A general consequence of using image plane scanning is that the field of view of the detector is moved across the entrance optics and sometimes across parts of the scanner casing as well. As a result, it is difficult to prevent some spurious signals from being introduced from this internal scan, particularly at thermal wavelengths where gradients of fractions of a degree may give rise to appreciable signals. On the other hand, it is probably possible to obtain higher duty cycles for short scans with image plane scanning than with object plane scanning. However, the prime reason for rejecting image plane scanners is that the object plane scanner described in the following section is simpler, particularly from a mechanical point of view, than any of the other relevant approaches of which we are aware.

Image plane scanners considered include the system referred to above, the corner mirror drum discussed in appendix IV, several more or less conventional scanners based on counter-rotating mirrors or prisms, and various fiber-optics scanning schemes. Prisms and fiber optics must, of course, be excluded for wide wavelength range systems due to the chromatic aberrations of the former and spectral absorption in the latter.

Of the object plane scanners, the conventional rotating single and multiple 45° mirror scanners are unsuitable because of low efficiency or large size. While an oscillating object plane mirror, such as the Hughes/ERTS scanner, appears to be practical, we have come to believe that a mirror nutating about a small angle presents the best solution. Although it would be somewhat less efficient than the proposed Hughes/ERTS scanner, the inefficiency is offset by much greater mechanical simplicity and, in particular, by the absence of nonuniform motion of any kind. The scan geometry is discussed in appendix III, and the recommended system is described in the following sections.

3.4.3. THE RECOMMENDED SYSTEM

No attempt has been made to carry out a detailed design, inasmuch as it is not practical to do so before the experiment carrier and orbital characteristics are known. However, one of the encouraging aspects of this approach is that because of the design's simplicity, it is possible to

determine its feasibility with considerable confidence without detailed study. While this is not an over-riding advantage, it is a considerable one if a short development time is required. Further, the design's simplicity is suggestive of high reliability.

A side-view schematic diagram of the proposed scanner is shown in figure 10. In the spectrometer section a dichroic mirror is used to separate the shorter wavelength channels from the thermal channel. A glass prism can be used to separate the remaining channels.

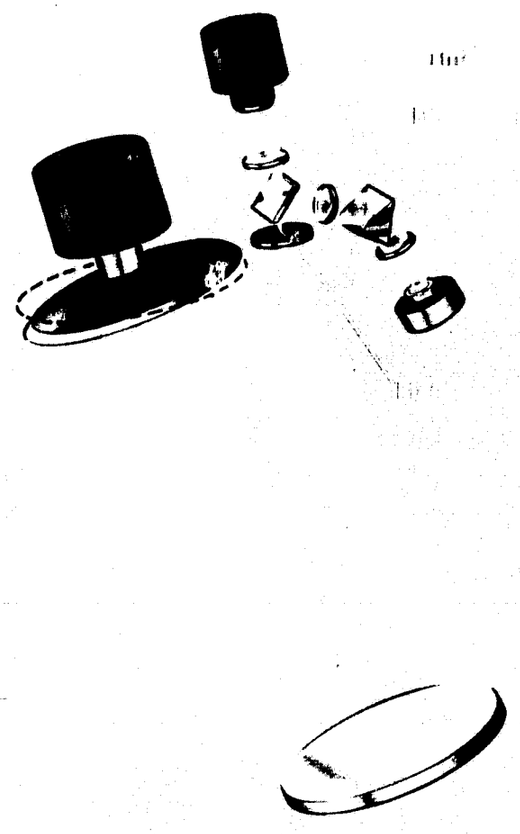

FIGURE 10. SCHEMATIC DIAGRAM OF PROPOSED SCANNER

Consider the following formula:

$$\delta\lambda = \frac{\beta D_1}{D_2(d\theta/d\lambda)}$$

where $\delta\lambda$ = spectral interval

β = angular resolution of scanner

D_1 = scanner aperture

D_2 = spectrometer beam cross-section

$d\theta/d\lambda$ = angular dispersion of prism or grating

This formula, derived in a previous program [14], shows that since a prism of modest size is acceptable for the recommended scanner, the spectrometer design should be straightforward. No specific recommendations are made for the limits of the spectral bands, but it is assumed that they would be similar to those originally proposed for the ERTS scanners:

Band 1	0.5 to 0.6 μm
2	0.6 to 0.7 μm
3	0.7 to 0.8 μm
4	0.8 to 1.2 μm
5	1.55 to 1.75 μm
6	2.2 to 2.4 μm
7 (thermal)	10.5 to 12.5 μm

Unlike that of the ERTS program, our thermal channel is spatially synchronous with the shorter wavelength channels. While the band limits need not be fixed until the detector arrays are ordered, appreciable reductions in spectral bandwidths could not be accepted because of adverse effects on performance. (NOTE: An airborne scanner, which can use an angular resolution an order of magnitude larger, has a considerable advantage over an orbital scanner in this respect.)

The collector mirror is shown as an off-axis paraboloid, and the angle between the paraboloid axis and the scan mirror drive shaft is made small to provide a compact system. A Cassegrainian collector might prove preferable in regard to control of aberrations, however, in which case a larger angle between the two axes might be preferred.

To remove most of the redundancy of the moving circular scan, only a little less than 1/3 of each scan pattern is used. To reduce the scan mirror rotation from 7200 rpm and to enhance the overall sensitivity, three detectors are used in each channel. These scan adjacent tracks, as shown in figure 11, and require that the entrance slit to the spectrograph have an aspect ratio of 3:1, so that the long dimension of the image at the ground lies parallel to the ground track. Optical separation of the three elements in each band thus depends on the optical performance of the scan mirror, collector, and spectrograph. However, since the f/numbers of the collector and spectrograph collimator can be made large, and since imaging is only required over a total angle of 4 mrad, no serious problem of implementation is foreseen in this respect.

The combination of the use of three detectors in each band with the use of a little less than 1/3 of each scan cycle enables the video data to be serialized in an efficient manner. This seri-

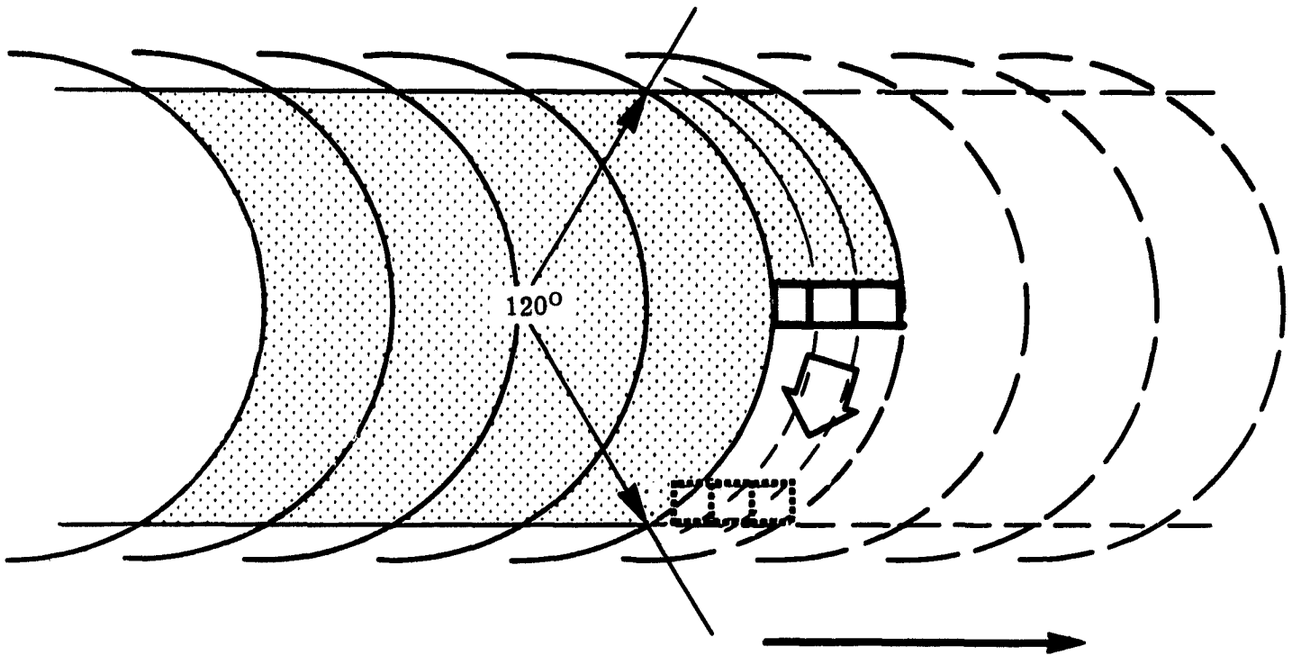

FIGURE 11. SCAN PATTERN OF PROPOSED SCANNER. Instantaneous scan circle: diameter = 76.4 mrad or 19 nmi.

alization would be accomplished by delaying the six or seven signals from each of the second and third scan lines by 120° and 240° respectively (then multiplexing all of the signals for telemetry on a single channel). The reformating could be done either by digitizing the signals and using conventional digital storage and readout techniques or by recording the signals on parallel tracks on a magnetic drum mounted on the same shaft as the scan mirror and then reading out at appropriate times. In either case, the important synchronization of the video signals for the various wavelength bands along each scan line can be preserved.

Calibration signals would be introduced by means of a mirror chopper in front of the spectrograph entrance slit. This chopper would be synchronized with or mechanically integrated with the scan mirror in such a manner that the calibration signals would occur during unused parts of each scan cycle. The signals would then be formated into appropriate times in the multiplexed output.

Some form of automatic gain control (AGC) and automatic level control (ALC) will be necessary. As explained in section 3.6, the problem of selecting an AGC/ALC system lies in selecting a philosophy rather than in implementing it. In this case, the relatively narrow swath width will reduce the probability of large changes in signal level along a single scan line. As a result, it should be practical to use a relatively straightforward system, either (1) preselecting gains and

levels on the basis of a priori knowledge of the area being overflown and its illumination, or (2) using a relatively conventional system based on the assumption that the mean signal level and its variance recorded during one set of scan lines is appropriate input information to set the gains and levels for the subsequent set of scan lines.

While the detailed specifications for the scanner must depend upon the experiment carrier and particularly upon orbital characteristics, a sample set of specifications is given below, based on the assumption that a circular orbit of 250-nmi altitude is used.

Provisional Specifications

Angular resolution	0.133 mrad
Resolution at ground	200 ft
Half angle of conical scan	38.2 mrad
Swath width	16 nmi
Number of elements in each scanned arc	550
Collector aperture	18 in.
Detector size at f/3.5	0.2 mm
Total onboard weight (excluding TM system or recorder)	≈450 lbs

Provisional Wavelength Band Designations

1. 0.5 to 0.6 μm
2. 0.6 to 0.7 μm
3. 0.7 to 0.8 μm
4. 0.8 to 1.2 μm
5. 1.55 to 1.75 μm
6. 2.2 to 2.4 μm
7. 10.5 to 12.5 μm

3.5. COMMUNICATION LINK FROM SATELLITE TO GROUND STATION

3.5.1. RADIO-FREQUENCY LINK

This section considers the requirements and specifications of the down-link telemeter that modulates the data signals from the scanner and transmits this information to the ground station. A brief history of spacecraft data links is given in appendix V, and useful general background can be found in reference 15.

In the proposed system it is assumed that the radio frequency (RF) carrier is within S-band (approximately 2300 Mc). This constraint on the RF channel is based on the following considerations:

(1) S-band lies well within the space window where propagation losses are minimal.

(2) Spacecraft and ground station equipment (such as antennas and transmitters) for S-band is readily available, and space communication systems within this band have been designed.

(3) Ground station coverage under the Space Tracking and Data Acquisition Network (STADAN) and the Manned Spaceflight Network (MSFN), which utilize S-band communications, gives extensive world coverage. (See appendix VII.)

(4) A high carrier frequency is necessary to accommodate the large data rates from the scanner.

The performance of a radio link between an orbiting satellite and a ground-based receiving station can be expressed by the ratio of the RF-carrier signal power (at the receiver antenna output) to the effective noise power (as a function of the link parameters) at the receiver input. This ratio is developed in the following discussion.

From fundamental propagation theory, the received power of the carrier at the receiver antenna can be expressed as:

$$P_r = \frac{P_T G_T}{4\pi d^2} \times A_R \qquad (1)$$

where P_r = carrier power received

P_T = power radiated from transmitting antenna

G_T = gain of transmitting antenna

A_R = effective area of receiving antenna

d = range

If the assumption is made that the receiving antenna is a parabolic reflector, the gain of the receiving antenna (G_R) is given by the following expression:

$$G_R = \frac{4\pi A_R}{\lambda^2}$$

where λ = wavelength of C/f

C = velocity of light

f = radio frequency

or

$$A_R = \frac{G_R \lambda^2}{4\pi} \qquad (2)$$

Substituting equation 2 in 1, the expression for the carrier power received becomes:

$$P_r = P_T G_T G_R \left[\frac{\lambda}{4\pi d}\right]^2 \tag{3}$$

The expression $\left[\frac{4\pi d}{\lambda}\right]^2$ is a measure of the free-space loss between two ideal isotropic antennas and is designated by L_{FS}. Therefore, equation 3 can be written:

$$P_r = \frac{P_T G_T G_R}{L_{FS}} \tag{4}$$

To obtain the desired S/N ratio, we express the noise power at the receiver input by the equation

$$N = KTB \tag{5}$$

where N = noise power

K = Boltzmann's constant

B = IR bandwidth

T = effective input noise temperature

The S/N ratio for the system can then be obtained by dividing equation 5 by equation 4.

$$\frac{P_r}{N} = \frac{P_T G_T G_R}{KTBL_{FS}} \tag{6}$$

In a practical system, additional carrier losses result from cable and equipment losses, and also, as a result of modulation, there is a loss of carrier power to the information sidebands. The total effect of these spurious power losses can be expressed as a degradation factor (D_f) from the ideal expression given by equation 6. The final P_r/N ratio can then be written as:

$$\frac{P_r}{N} = \frac{P_T G_T G_R}{KTBD_f L_{FS}} \tag{7}$$

It is convenient to express the terms in equation 7 in decibels, in which case:

$$\frac{P_r}{N}(db) = P_T + G_T + G_R - D_f - KTB - L_{FS} \tag{8}$$

Each term of equation 8 is considered below, and specific values are assigned which establish the design of the proposed system.

Transmitter Power (P_T). It is assumed that the available power to the transmitting antenna is 20 w or 13 dbw. This power figure is based on the design of current communication systems that have been implemented for near earth-orbiting satellites. (See appendix VI.)

Transmitter Antenna Gain (G_T). In order to avoid antenna alignment and pointing errors, it is assumed that the transmitting antenna is isotropic, radiating equally in all directions with an efficiency of 0.6. Therefore, G_T can be expressed as $G_T = 10 \log 0.6 \cong -2$ db.

The Receiving Antenna (G_R). The receiving antenna considered in the communication link is a 30-ft parabolic reflector with a gain of 44 db (including the feed and polarization losses). This antenna is a standard unit used throughout the MSFN ground station system. (See appendix VII.)

Effective Input-Noise Temperature (T). The effective system temperature for the 30-ft receiving antenna and input amplifier (antenna pointing toward horizon and using amplifier and uncooled parametric device) is 355°K. The effective noise density for this temperature can be written 10 log KT = -203 db/Hz.

Free-Space Loss (L_{FS}). The free-space loss L_{FS} has been defined and can be expressed as:

$$L_{FS} = \left[\frac{4\pi d}{\lambda}\right]^2$$

Free-space loss can be written in logarithmic form and becomes

$$L_{FS} = 36.6 + 20 \log f + 20 \log d \qquad (9)$$

where f = MHz

d = statute miles

The value for the distance (d) is obtained from the expression that relates slant range to the satellite orbital distance and to the elevation angle of the receiving antenna.

This equation is

$$d = (R + h)\frac{\sin\left[\frac{\pi}{2} - \alpha - \sin^{-1}\frac{R}{R+h}\cos\alpha\right]}{\cos\alpha}$$

where R = radius of earth

h = satellite orbit above earth surface

α = elevation angle of receiving antenna

In an extreme case for h = 250 miles, $\alpha = 8^\circ$ above the local horizon, d ≅ 1000 miles.

A value for the free-space loss can now be obtained from equation 9 using f = 2300 Hz and d = 1000 miles. With these values, $L_{FS} \cong 164$ db.

Degradation Factor (D_f). From experience gained in previously designed S-band communication links, it is anticipated that the degradation factor will be of the order of 4 db.

Signal-to-Noise (P_r/N). If the carrier is modulated by some form of angle modulation, then the minimum S/N ratio for threshold is approximately 12 db. For the proposed system a conservative design with a carrier margin of 12 db is considered. This gives a desired P_r/N ratio of 24 db.

In the previous discussion, values for the different terms of equation 7 have been designated except for the receiver intermediate frequency (IF) bandwidth. The value for the available receiver bandwidth (B) is obtained by solving equation 7 for B, substituting the values for the different terms as previously prescribed. This results in:

$$B(db) = 66$$

or

$$B \cong 4.0 \times 10^6 \text{ Hz}$$

The IF bandwidth for a modulation system generally contains symmetric sidebands of information; therefore, the information bandwidth or baseband is 1/2 of the IF bandwidth. In the communication system being considered, this available bandwidth is, then, 2 MHz.

From equation 8 it is apparent that the available baseband for the system could be increased by modifying one or several of the system's parameters. For example, if the satellite's transmitting antenna were the higher-gain antenna of the Apollo system rather than the isotropic Apollo antenna, then the available information bandwidth would be 15 MHz. This change in the transmitting antenna would require, however, a system for antenna alignment, since the higher gain (7 db) antenna has a beam width of 68^o. An increase in baseband could also be realized by using a cooled parametric amplifier as the receiver input stage. This introduces an effective noise temperature of 100^oK, which produces an effective information bandwidth of 5 MHz.

Future development in satellite communication equipment will certainly improve the efficiency of the data link. It is anticipated that in the next few years, 50 w of power will be available for spacecraft communications, and with the progress that is being made in receiver design and modulation techniques, a much smaller carrier margin will be required (ref. 16).

From the analysis of the radio frequency requirement, it was shown that 2 MHz of baseband was available for the data signals of the scanner. In section 3.5.2 several methods for multiplexing this information are considered, and for each method a maximum per channel bandwidth is derived.

3.5.2. MULTIPLEXING SYSTEMS

Several studies (refs. 17, 18) have attempted to compare the efficiency of different multiplexing and modulation systems on the basis of relative carrier power and reception bandwidth required to transmit a fixed information bandwidth. The results of these studies indicate that for medium accuracy systems (>1%), PAM-FM modulation has a distinct advantage over other

methods in required bandwidth and power. To obtain errors lower than 1% with PAM-FM, the bandwidth and power must be increased to a point where a PCM-FM system becomes superior.

At the present time, however, existing PAM systems are designed for low to medium bandwidth applications, and for wideband data transmission, FM-FM or PCM-FM modulation techniques are generally used. For this reason, the following discussion considers the bandwidth limitations imposed when the information from the scanner's 7 channels is multiplexed via PCM and FM onto the available baseband of 2 MHz. It is conceivable, however, that in the near future PAM-FM systems which fully utilize their theoretical advantages will be available for multiplexing wideband data.

FM Multiplex System. A recent study (ref. 19) has shown that a conservative design (acceptable S/N ratio and interchannel cross talk) for a constant bandwidth FM system for wideband application can be realized with the following specifications:

$$\text{modulation index } (m) = 2^*$$

$$\frac{\text{FM Bandwidth}}{\text{Guardband}} = \frac{(BW)_{FM}}{GB} = K$$

where K = a constant with approximate value of 1.25. From Carson's rule for FM modulation, the FM bandwidth is given by:

$$(BW)_{FM} = 2(m + 1)f_i \tag{10}$$

where f_i = frequency content of the information.

For the case where m = 2, equation 10 becomes:

$$(BW)_{FM} = 6f_i \tag{11}$$

If n channels of information are multiplexed onto a finite baseband (W) with guard bands spaced between the channels, then the equation that expresses the complete packing of the information onto W is given by:

$$n(BW)_{FM} + \left[\frac{(n - 1)}{K}(BW)_{FM}\right] = W \tag{12}$$

In the specific case for the multispectral scanner where n = 7 and $W = 2 \times 10^6$, using a value of 0.8 for K, equation 12 becomes:

$$7(BW)_{FM} + 4.8(BW)_{FM} = 2 \times 10^6 \text{ Hz}$$

or

*This modulation index of 2, in fact, is a recently adapted Inter-Range Instrumentation Group standard for constant bandwidth FM systems.

$$(BW)_{FM} = 170 \times 10^3 \text{ Hz} \tag{13}$$

If the value for the FM bandwidth as given by equation 11 is now substituted in equation 13, the frequency bandwidth for each channel that can be handled by the given amount of baseband can be obtained. That is,

$$6f_i = 170{,}000 \text{ Hz}$$

or

$$f_i = 28{,}000 \text{ Hz}$$

Pulse Code Modulation (PCM). In a PCM system each channel is interrogated in turn, digitizing the value of the channel. The result is a pulse train of bits that represent the coded information of the data. If the highest frequency component for each channel is f_s, then in order to sample each channel at the Nyquist rate of two samples per cycle of f_s, the throughput rate for the multiplexer of a 7-channel system would be $7 \times 2 \times f_s = 14f_s$ samples/sec. To maintain an accuracy in the transmission of the data of 1/2%, the information should be encoded with at least eight binary bits. For the 7-channel system, this would give a pulse train at the output of the multiplexer with a frequency of $112 \times f_s$ bits/sec. It is known from information theory that the bandwidth required of a communication link to pass information at this rate is:

$$\frac{112xf_s}{2} = 56f_s \text{ Hz}$$

For this information to be accommodated by the available baseband of 2×10^6 Hz, the following equations hold:

$$56f_s = 2 \times 10^6 \text{ Hz}$$

or

$$f_s = 36 \times 10^3 \text{ Hz}$$

This value for the maximum frequency capability of each channel is based on the assumption that the information is sampled at the Nyquist rate. For scanning data that represents some visual scene, this scanning rate might prove to be inadequate. Any increase in the sampling would decrease the available information bandwidth per channel that the system could handle.

3.6. SIGNAL HANDLING

3.6.1. POSSIBLE MODES

Signal handling is defined here to be the automatic adjustment of the electronic gain, the electronic offset, and the calibration source-radiance settings. The adjustment of gain, offset,

and source radiance of each channel or source can be based either upon the target signal, the source signal, or a programmed value. Generally, all singular combinations of these are considered. The various modes are listed in table III. Some of the combinations are pointless, and some are not practical; however, for completeness all are considered. The gain and offset adjustments are considered inseparable; that is, if the setting of one is changed, the other must in general be changed too. The two adjustments are separable only in a special reflective-data

TABLE III. ADJUSTMENT BASIS

Mode	Adjustment Function	Basis for Setting Adjustment Function
1	G&O	P
	R	P
2	G&O	P
	R	S_t
3	G&O	P
	R	S_s
4	G&O	S_t
	R	P
5	G&O	S_t
	R	S_t
6	G&O	S_t
	R	S_s
7	G&O	S_s
	R	P
8	G&O	S_s
	R	S_t
9	G&O	S_s
	R	S_s

Definitions — Adjustment Functions

G = Video gain, the peak-to-peak video signal divided by the peak-to-peak apparent radiance

O = Video offset, the voltage added to one of the signal extremes to be recorded that will position the signal extreme at the edge of the dynamic range

R = Apparent radiance from the reference source

Definitions — Setting Basis

P = Preset or programmed adjustments set by command

S_t = Video signal from the target or scene

S_s = Video signal from a reference source

case in which zero radiance is represented by a video signal of 0 v. In such a special case, if dc coupled or restored electronics are used, the gain adjustment can be set by any means desired, and the offset need not be adjusted.

Mode 1. In this mode the gain, offset, and source radiance are preset or programmed. Although this mode is simple to implement and basically reliable, it has the following problem areas:

(1) Slight changes in target radiance, detector bias, detector responsivity, electronic gain, or electronic drift from that expected can cause an incorrect range of target radiance to be recorded.

(2) A priori knowledge is required.

(3) Programming commands to the satellite from a ground station are required prior to a data run.

Mode 2. The gain and the offset adjustments are preset. This means that the dynamic range is preset, and therefore this mode has the same problems as mode 1. The target signal will give no additional information on the proper setting of the radiance of each reference source, and as a result, this mode is less satisfactory than mode 1.

Mode 3. The gain and offset, and therefore the dynamic range, are preset in this mode. The reference-source radiance is controlled by the source signal, which implies that the source radiance can be more accurately known from the source signal than from the source-radiance setting. If this were so, the target signal could be accurately used to determine the apparent target radiance, and no reference sources would be needed.

In practice, however, reference sources are in fact needed, and in addition, in most multispectral radiometry the absolute radiance in each channel isn't as important as the relative difference in radiance between channels. This fact can be most accurately established by viewing the same sources by as many spectral channels as possible. Reference sources are, therefore, used on most multispectral sensors where quantitative data is desired in addition to good pictures. Clearly, then, mode 3 has no value.

Mode 4. The source radiance is preset or programmed in this mode, and the gain and offset (or dynamic range) are set according to the signals from the scene that is being remotely sensed. This is a good mode to operate in a substantial number of cases. The dynamic range is optimally set by a preset decision rule (see sec. 3.6.3) to get the most desired scene information from the sensor signal. Since source radiance is preset, it neither has to operate over a wide range nor rapidly change its radiance. As a result, a more accurate and reliable radiance can be obtained. The basic linearity of the sensor is assumed when two sources are used to establish the relationship between the scene radiance and the resulting video signals. However,

valid calibration can be established even when the sensor is nonlinear, if the nonlinearity is known and is stable. This mode presents a problem, although solvable, in that if the required dynamic range of the target signals is either very large or very small compared to the difference between the two source radiances, the source signal is either beyond the dynamic range of the system or is hidden in the noise respectively. (This is possible if the dynamic range to noise level of the scanner is larger than the dynamic range to noise level of the data link). Considerable offset could also be present. This can be solved by deriving electronically a pseudo source signal from the source signal itself by adding gain or attenuation and offset. The question of whether to use continual or periodic updating with infinite or finite resolution in setting the gain and offset on the scene signals and on the pseudo source signals is considered in subsection 3.6.4.

The use of a separate sensor to prescan the scene and a similar approach of delaying the normal sensor output with a memory in order to allow time to make a good decision on what the gain and offset settings should be is considered in subsection 3.6.5 which deals with the implementation considerations of mode 4.

Mode 5. This mode is similar to mode 4 except that the target signal is used to set the source radiance. It is also similar to that used in the present University of Michigan C-47 system in which the source radiance and dynamic recording range are controlled manually. One problem with this system is that the sources must maintain their accuracy over the extreme radiance ranges from all scenes, which is most difficult for source blackbody temperatures below the dew point. Also, the source radiance must change as fast as the scene radiance, a requirement that is more of a problem from a satellite than from an aircraft. Thus, while mode 5 is satisfactory for a manual system, for an automatic satellite system, mode 4 is probably superior.

Mode 6. This mode is similar to mode 4 except that the reference-source radiance is set by the signal when the reference source is being viewed. As explained for mode 3, such a procedure eliminates the need for reference sources, and this mode is, therefore, considered inconsequential.

Mode 7. The dynamic range of the recording system is set by the source radiance, and the references are preset for mode 7. This mode of operation has also proven satisfactory for certain runs for The University of Michigan C-47 system. The dynamic range for the solar-reflective spectral bands has been set to record a previously chosen range of reflectance based on the reflectance source (diffuse solar illumination). The dynamic range for the thermal-emitting spectral bands has been set to record a previously chosen range of apparent temperatures based on the thermal reference sources. This mode is practical only if considerable current ground-truth and planning information is available for each section of data collection. It is not considered practical for most satellite missions.

Mode 8. Mode 8 is similar to mode 7 except that the source radiance is set in relation to the target radiance. The mode has the same problems of dynamic range and rate of change of the sources as mode 5 and is, therefore, inferior to mode 4.

Mode 9. Mode 9, like modes 3 and 6, has no need for reference sources and is again considered inconsequential.

3.6.2. SELECTION OF PREFERRED MODES

Mode 4 appears to be the most practical automatic gain and level control for a multispectral sensor, although modes 5, 7, and 8 have some advantages under certain conditions. The radiance from the sources can either be preset or set relative to the target signal. If set relative to the target signal, the accuracy of the source radiance is hard to maintain because of the dynamic range and speed of response required.

The gain and offset can be set relative to the source radiance or relative to the target signal. If the source radiance is preset because of the source-accuracy problem, and if the gain and offset are set according to the source radiance, then the gain and offset are really also preset. Therefore, either considerable current ground-truth information and close ground-to-satellite control is required, as in mode 7, or the gain and offset are set relative to the target signal, and the sources are preset as in mode 4. Mode 4 appears to be the most practical for a satellite.

3.6.3. DYNAMIC RANGE SELECTION

If the dynamic range of the video signal exceeds that of the data link and recording system, it will be desirable to use some control law on which to base the gain and level selection. Three control laws which might be used are:

(A) The maximum limit of the signal's dynamic range is exceeded by X% of a particular previously scanned area, and the minimum limit is exceeded by Y% of the area.

(B) The center of the dynamic range is set at the center of extreme limits of the signal over a particular previously scanned area. The limits of the dynamic range are set at a certain percentage (can be larger or smaller than 100%) of the extreme limits of the signal over the same previously scanned area.

(C) The center of the dynamic range is set at the average signal level, and the limits of the dynamic range are set at a factor times the average rms ac value of the signal.

Each of the above control laws can be updated (a) at regular periodic intervals, (b) continually, or (c) whenever the discrepancy between the desired and actual setting exceeds a threshold. Each setting range could be in finite or infinite steps.

3.6.4. GAIN AND OFFSET ADJUSTMENT PHILOSOPHY

The question of using continual or periodic updating should be considered with regard to the processing and analysis of the data, the ease of implementation, and the aesthetic appeal of the imagery. Analyzing data that has continually-changing gain and offset would be difficult; the processing equipment would become more complex, and the accuracy of the data would decrease. Implementing the continually-changing automatic gain control in the sensor is relatively easy; however, when the requirement to know the gain and offset is presented, periodic updating becomes attractive. Also, the aesthetic appeal of the imagery cannot be ignored. If a signal representing the radiance of a river or lake is continually changing, when it wouldn't be to a human observer, confidence in the system is lost. The ideal system, in the authors' opinion, therefore, should have periodic rather than continual updating.

One also must decide whether to use finite or infinite resolution in setting the gain and offset. Although perhaps slightly more difficult to implement, finite gain settings have the advantage in that slight variations in the scene would not cause slight changes in gain and offset. Continuous changes would result in poor imagery, unless compensated. Also, with finite resolution gain and offset changes would be obvious in the imagery. (The actual knowledge of the gain and offset values is not required except to diagnose equipment problems, if the reference signals are recorded and if the gain and offset aren't changing and are approximately correct.)

In order to determine the best dynamic range (gain and offset), a significantly large area in the scene must be examined. A significantly large area here is assumed to be one in which the apparent radiance is generally spatially homogeneous and in which the gain and offset settings should remain unchanged. Since the orientation of the scene is generally random with respect to the scan direction, the dimensions of this significantly large area should be generally equal in the direction across the scan and parallel to the scan.

3.6.5. IMPLEMENTATION CONSIDERATIONS OF MODE 4

Figure 12 shows a scene sketch and the resulting imagery of two implementations of mode 4. The scene is made up of water and land. We have assumed here that there is only one optimal dynamic range for all the land and another for all the water. It is also assumed that a decision can be made electronically, based on the signal that has been received over a previously scanned area. In Implementation A (fig. 12) the dynamic range recorded for area A2 was determined on the basis of the signal from A1, and similarly, the range for A3 was based on A2. It can be seen that the dynamic range is not optimally set for either A1, A2 or A3. Implementation B (fig. 12) utilizes the same concept with constant dynamic range in smaller areas. The areas are defined by the first digit representing the column, and the remaining digits representing the row. For example, the dynamic range for area B47 would be determined from the signal from B46. The signal from B46 is made up of certain segments of several lines, and a decision can be made

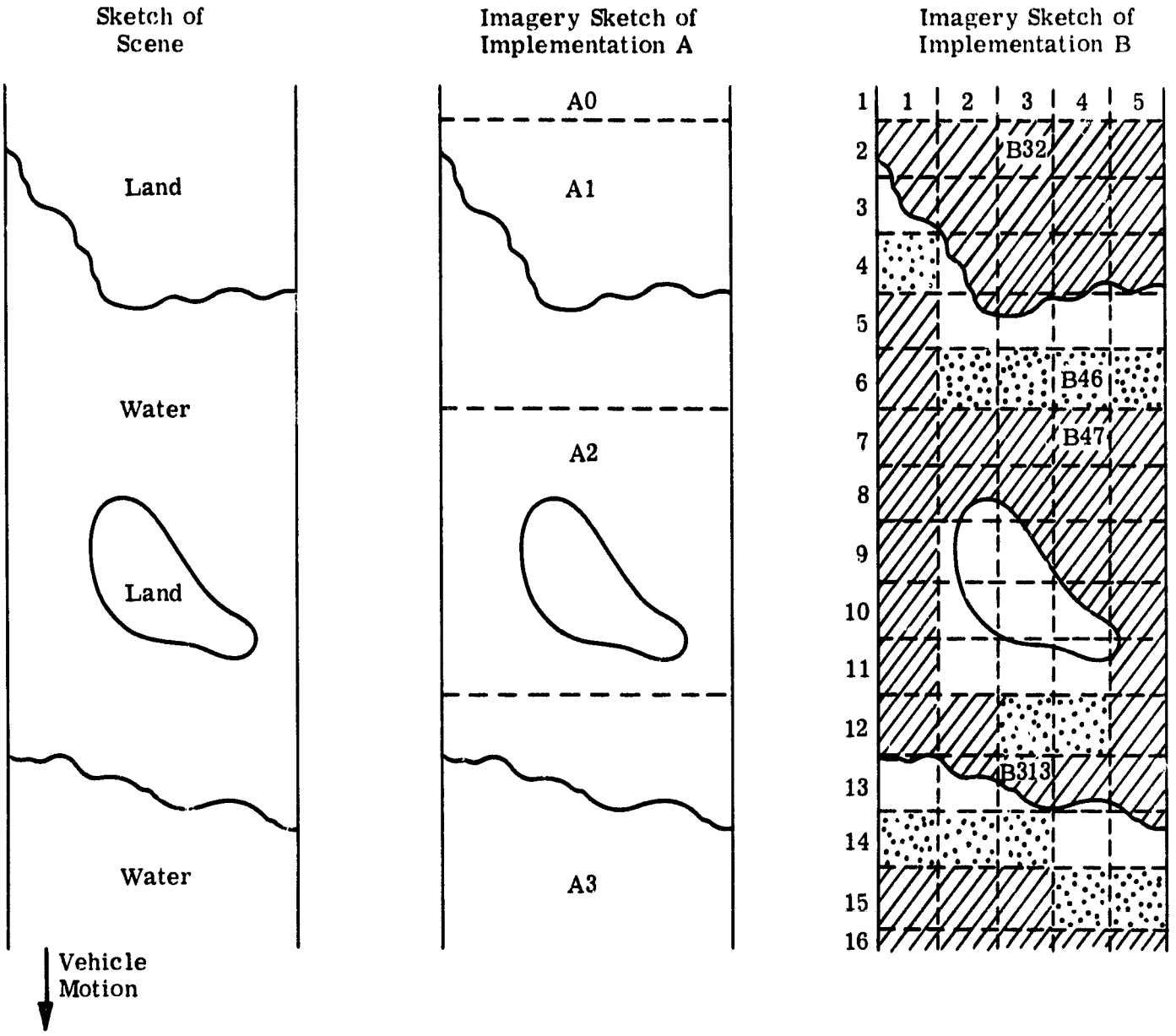

FIGURE 12. MODE 4 IMPLEMENTATIONS

using any of the decision rules listed in section 3.6.3 or by other similar criteria. The cross-hatched areas in figure 12 are those which have the optimal dynamic range recorded. The water-land boundaries present a problem of determining the best dynamic range; however, a lot of the area can have the dynamic range set optimally with Implementation B. The dotted areas are the additional areas that would have the optimal dynamic range recorded, if the decision is based on a prescanned signal or on a stored signal of the area. Both these techniques are, however, somewhat unreliable and expensive to implement and therefore not considered practical.

Figure 13 is a block diagram of Implementation B, and figure 14 contains a definition of terms and waveforms for it. The AGC and ALC equipment required for Implementation A is the

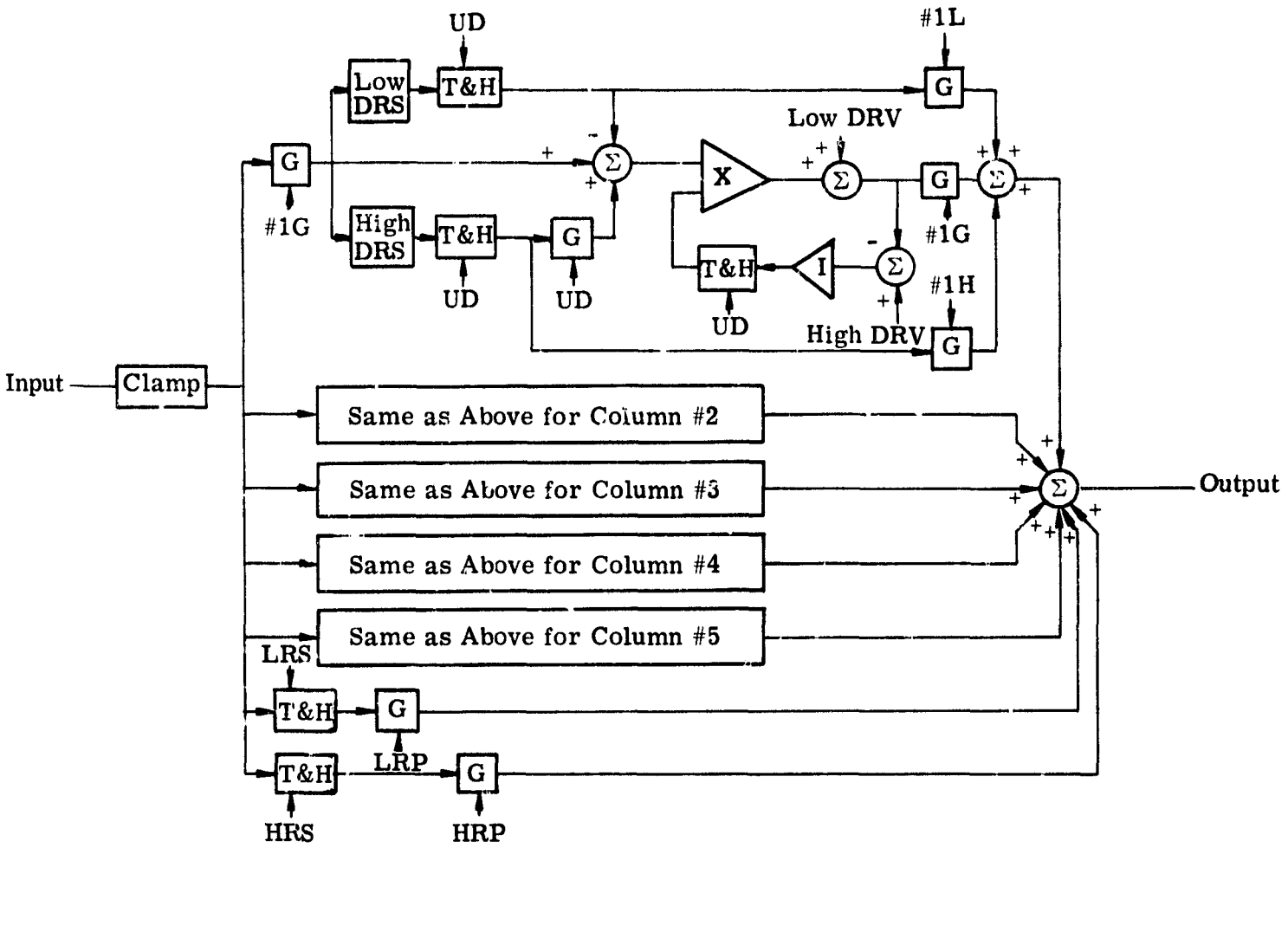

FIGURE 13. ACG AND ALC DIAGRAM OF IMPLEMENTATION B OF FIGURE 12

same as that required for column 1 of Implementation B (see fig. 13). If the scene (fig. 12) is divided into 75 small areas, Implementation A had the dynamic range improperly set for all these areas, while Implementation B had the proper dynamic range for 38 of them (cross-hatched). If the dynamic range had been based on prescanned signals or on stored signals, 12 more areas, or a total of 50 of the 75, would have had the proper dynamic range. The implementation would include that required for Implementation B and, in addition, either another detector and preamp with gating electronics or a storage device.

In the authors' opinion, Implementation B is a good compromise for most cases. The equipment described above is based on one spatial or spectral channel. For a realistic system with multispectral and multispatial detector arrays, the amount of equipment required to set the dynamic range properly gets relatively large, but up to 100-element array systems would seem practical with state-of-the-art equipment.

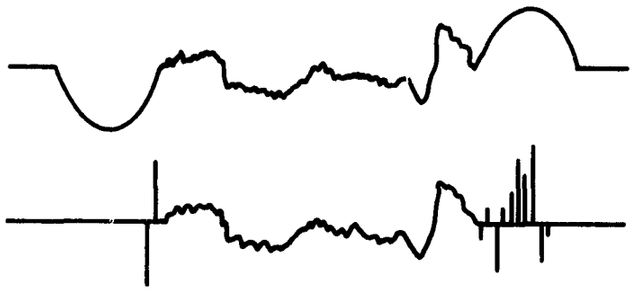

Typical Input

Output for Typical Input

Gate Identification

Abbr.	Description
#1G	Column #1 Gate
#2G	Column #2 Gate
#3G	Column #3 Gate
#4G	Column #4 Gate
#5G	Column #5 Gate
#1L	Column #1 Low Dynamic Range Sensor Print Gate
#1H	Column #1 High Dynamic Range Sensor Print Gate
#2L	Column #2 Low Dynamic Range Sensor Print Gate
#2H	Column #2 High Dynamic Range Sensor Print Gate
#3L	Column #3 Low Dynamic Range Sensor Print Gate
#3H	Column #3 High Dynamic Range Sensor Print Gate
#4L	Column #4 Low Dynamic Range Sensor Print Gate
#4H	Column #4 High Dynamic Range Sensor Print Gate
#5L	Column #5 Low Dynamic Range Sensor Print Gate
#5H	Column #5 High Dynamic Range Sensor Print Gate
LRS	Low Reference Sample Gate
HRS	High Reference Sample Gate
LRP	Low Reference Print Gate
HRP	High Reference Print Gate

Code: DRV = Dynamic Range Voltage
DRS = Dynamic Range Sensor
T&H = Track and Hold
G = Gate
Σ = Summator
I = Integrator
x = Multiplier

Clamp dc restoration
UD Command pulse to update the ALC and AGC (typically once each 100 scans)

Note: The voltages from the references are assumed to have a preset gain and offset added in their T&H modules.

FIGURE 14. TERMS AND WAVEFORMS IN FIGURE 13

3.6.6. MODE 4 — AGC AND ALC CIRCUIT DEVELOPMENT

The goal of this circuit is to set automatically the gain and offset, so that two specific input voltages will be set at the extremes of the dynamic range in the telemetry link. Since the system is assumed to be linear, the input-output relationship must be a straight line as shown in figure 15.

The equation of the line that passes through the two known points is:

$$\frac{y - y_1}{x - x_1} = \text{slope} = \frac{y_2 - y_1}{x_2 - x_1}$$

or

$$y = (x - x_1)\frac{y_2 - y_1}{x_2 - x_1} + y_1 \tag{14}$$

where x = the input

y = the output

x_1 and x_2 = extreme values of the input

y_1 and y_2 = predetermined dynamic range extremes of the output

One circuit, shown in figure 16, will compute the slope if the following conditions are met:

(1) The external input to the multiplier must be forced to be $x_2 - x_1$.

(2) The multiplier output must be forced to be $y_2 - y_1$.

(3) The feedback (blank) box must be stable and provide for a high loop gain.

These conditions can be maintained by the circuit shown in figure 17, where A is a high-gain amplifier (an operational amplifier). Since the gain is high and the output finite, the input will be negligible. The dc-loop phase through the multiplier, the summer, and the operational amplifier must be negative in order for the loop to be stable, and this is accomplished by the negative sign on the second summer input from the multiplier. The frequency-rolloff characteristics of the combined multiplier, summer, and operational amplifier are assumed to be satisfactory for a stable loop. Since the loop is assumed to be stable, and since the output of the second summer is servoed to 0, the total inputs to this summer must be 0, and therefore, the multiplier output is $y_2 - y_1$. The external input to the multiplier is forced to be $x_2 - x_1$. Now all the conditions imposed in figure 16 are met by figure 17, and the slope is computed.

It is desirable to use the same basic circuit to compute y. This can be accomplished, as shown in figure 18. As a word of explanation, the track and hold module (T&H) is a device which has two states of operation as controlled by an electronic signal (in this case z). One state (track) is similar to an amplifier with a finite gain (usually one), and the other state (hold) is similar to a storage device in which is stored the last voltage level in the track mode prior to switching to the hold mode. A gate (G) is a device which also has two states of operation controlled by an electronic signal (z). In one state the gate has a gain of one from the input to the output, while in the other state there is no coupling or gain from the input to the output.

The slope-computing circuit of figure 18 has two modes of operation. The figure shows the first mode computing the slope, after having received the z signal, so that the gate has a gain of one and the T&H has a gain of one. x is assumed to be 0 during this time. The top input of the multiplier is, therefore, $x_2 - x_1$. Since the loop is closed through the T&H module, the A amplifier input must be 0, and therefore y must be y_2, making the multiplier output $y_2 - y_1$. For the

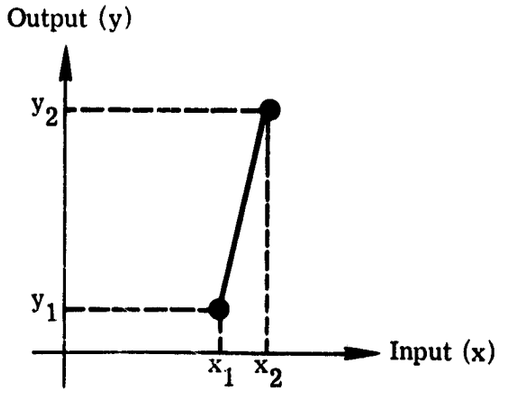

FIGURE 15. INPUT-OUTPUT RELATIONSHIP

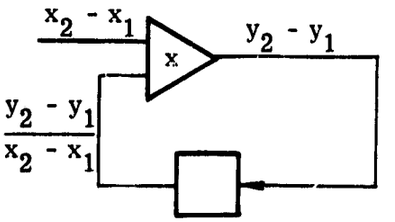

FIGURE 16. SLOPE-COMPUTING CIRCUIT

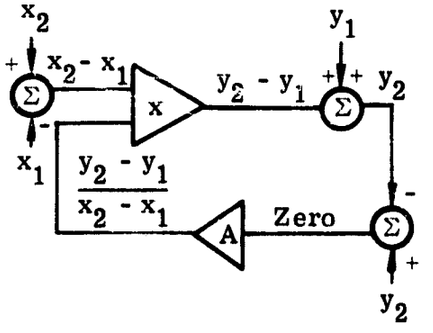

FIGURE 17. DETAILED SLOPE-COMPUTING CIRCUIT

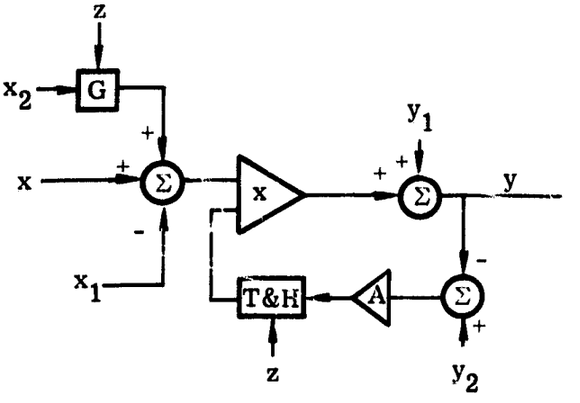

FIGURE 18. ALC-AGC CIRCUIT

multiplier to operate properly, its other input must be at $y_2 - y_1/x_2 - x_1$, i.e., the slope. The speed of this operation depends on the frequency response of the loop and can easily be less than a few μsec. The mode can then be switched by the electronic signal z, causing the gate gain to be 0 and the T&H module to go into the hold state. The T&H module will hold the value of slope stored. Now the top input to the multiplier is at $x - x_1$, and the output must be at $x - x_1(y_2 - y_1/x_2 - x_1)$. With the addition of y_1 to this, we obtain y as given in equation 14.

In summary, x and y are the input and output respectively. y_1 and y_2 are the predetermined dynamic range extremes of the output. x_1 and x_2 are the extreme values of the input desired to define the dynamic range to be telemetered. z is the mode-switching signal. Although other circuits can be constructed to perform this operation, this circuit is simple and has basic accuracy associated with closed-loop operation.

4
CONCLUSIONS AND RECOMMENDATIONS

The principal conclusion of this study is that a 7-band scanner with a ground resolution of 200-300 ft over a swath width of 15-35 nmi is the optimum system compatible with a single S-band telemetry system for early earth-orbiting experiments in the Apollo Applications Program. Our principal recommendation is that such a scanner system be developed and deployed at the earliest opportunity. We also recommend that further studies be directed toward the development of specific spacecraft scanner systems as well as toward development of subsystems and components (such as cryogenic systems or preamplifiers), where the research can usefully be performed without reference to a specific set of ground rules.

Although not a concern of this study, we also take the opportunity to point out that orbital scanners will be capable of producing volumes of data, beyond the scope of existing data-processing equipment. Therefore, we recommend further study of theories and methods of data processing. New methods of processing large quantities of data should be developed; then, in order to determine their relative validity and feasibility, they should be tested on data already collected by airborne systems.

Appendix I
Ge:Hg DETECTOR — PREAMPLIFIER LIMITATIONS: BACKGROUNDS BETWEEN 10^{15} AND 10^{18} PHOTONS-sec^{-1}-cm^2

Figure 19 is an equivalent circuit of a typical above-average Ge:Hg detector, while figure 20 shows this equivalent circuit coupled with a load resistor and preamplifier. The active element of the first stage of the preamplifier is assumed to dominate the amplifier noise. We assume also that a network which compensates for the capacitive loading on the detector follows the amplifier. (Table IV is a symbols list for the figures and the equations found in this section.)

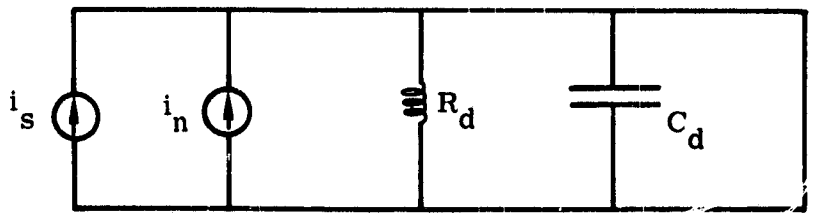

FIGURE 19. Ge:Hg DETECTOR EQUIVALENT CIRCUIT

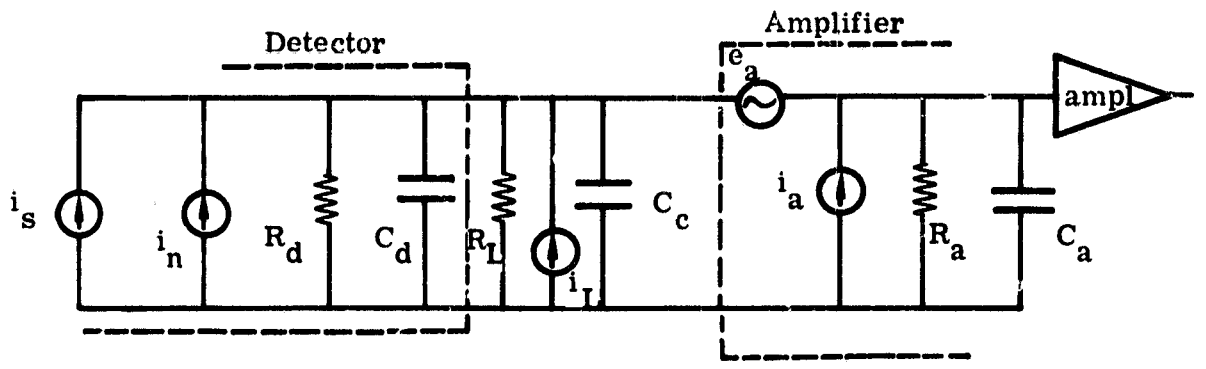

FIGURE 20. Ge:Hg DETECTOR WITH BIAS AND PREAMPLIFIER AC EQUIVALENT CIRCUITS

In an ideal detector-preamplifier system, the detector noise i_n should be higher than any other noise, and the S/N ratio out of the preamplifier (signal from i_s to the noise from i_n) should be as high as possible. Since i_s and i_n follow the same circuit path, only i_n will be considered with respect to the other noises. By taking Thévenin's equivalent, e_a can be referred to the other noise. The equivalent current i_e due to e_a is:

TABLE IV. SYMBOLS LIST FOR APPENDIX I

ampl Noiseless amplifier

C_a Amplifier input capacitance, pf

C_c Detector cable capacitance through Dewar and to an external preamplifier, pf

C_d Detector-element capacitance, pf

e_a Amplifier noise with the input connected to a short circuit referred to the amplifier input, v - $Hz^{-1/2}$

i_a Amplifier noise with the input connected to an open circuit referred to the amplifier input, amp - $Hz^{-1/2}$

i_e The equivalent current due to e_a, amp - $Hz^{-1/2}$

i_L Johnson noise from the load resistor, amp - $Hz^{-1/2}$

K Boltzmann's constant, $1.38 \times 10^{-23} v^2$ - $^oK^{-1}$ - Hz^{-1}

R Resistance, 10 megohm

R_a Amplifier input resistance, ohm

R_L Load resistor, ohm

T Temperature, ^oK

R_d Detector resistance = $\frac{1}{qMn\tau_r J_b}$ (assuming a square detector), which can be further reduced to $\frac{250\ K\Omega \times 10^{-17}}{j_B}$ (assuming that the detector is ohmic), ohm

where q = charge per carrier, coulomb-$carrier^{-1}$
n = quantum efficiency, carrier-$photon^{-1}$
J_b = incident background flux density below detector cutoff wavelength, photon-cm^{-2}-sec^{-1}
A = effective area of the detector, cm^2
τ_r = lifetime of the free carriers, sec
M = mobility of carriers, v^{-1}-sec^{-1}-cm^2

i_n = rms detector noise = $\frac{2V_c qM\tau_r}{(\tau_r S + 1)}\sqrt{\frac{nJ_b}{A}}$, which can be further reduced to $1.78(10^{-22})\sqrt{J_b/A}$ (assuming that 1/f noise and Johnson noise are negligible), amp-$Hz^{-1/2}$

where V_c = dc-bias voltage across the detector, v
S = Laplace transform

i_s = rms detector signal = $\frac{V_c qMn\tau_r J_s}{\tau_r S + 1}$ (assuming that the signal flux is small compared to the background flux), which can be further reduced to $2 \times 10^{-20} J_s A$ (assuming that τ_r is much less than the extrinsic (RC) time constant and therefore zero), amp

where J_s = incident signal-flux density below detector cutoff wavelength, rms, photons-cm^{-2}-sec^{-1}

$$i_e = \frac{e_a}{R_d||C_d||R_L||C_c}$$

where || means "added in parallel with." Now all current sources (i_s, i_n, i_L, i_a, and i_e) can be added vectorially since they go through the same circuit path. We will consider the worst case likely to be met, i.e., one with a background flux of 10^{15} photons-sec^{-1}-cm^{-2}. The area of the detector is assumed to be 10^{-4} cm^2. i_n is, therefore, $(1.78) \times (10^{-22})\sqrt{10^{+19}} = (5.61)10^{-13}$ amp-Hz$^{-1/2}$. The Johnson noise current (i_L) for the load resistor is $\sqrt{\frac{4KT}{R_L}}$. The resistor must be cooled to make the noise negligible for reasonable values of load resistance. With the resistor operating at the temperature of the detector (4°K), a load resistance of 1 megohm results in $i_L = 1.5 \times 10^{-14}$ amp-Hz$^{-1/2}$. A 2N4867A field-effect transistor (FET) is assumed to cause the noise in the amplifier. The specifications state that if the transistor is connected to a 10-megohm resistor (R), the total transistor noise (current plus voltage) is less than the resistor's thermal noise. The specifications further state that the transistor's voltage noise (e_a) is less than 10^{-8}v-Hz$^{-1/2}$. This can be stated mathematically as follows:

$$\frac{e_a^2}{R} + i_a^2 R < 4KT = 1.6 \times 10^{-20}\text{w}$$

Thus, the transistor's voltage-noise power plus its current-noise power is less than a 10-megohm resistor's thermal-noise power. The transistor's voltage noise power can be determined from:

$$\frac{e_a^2}{R} = \frac{(10^{-8})^2}{10^7} = 10^{-23}$$

which is negligible. Therefore,

$$i_a < \sqrt{\frac{1.6 \times 10^{-20}}{10^{-7}}} = (4)10^{-14}\text{amp-Hz}^{-1/2}$$

$$i_a \lesssim (4)10^{-14}$$

The effect from e_a is the worst at high frequency, where the capacitive impedance across the amplifier input is lowest. The capacitance ($C_d + C_c$) is 15 pf. At 1 MHz this is an impedance of about 10 kilohm. e_a at 1 MHz is less than $(2.5)10^{-9}$v-Hz$^{-1/2}$, which results in $i_e = (2.5)10^{-13}$. Of the two transistor noises i_e and i_a, the larger is i_e, which is approximately half the detector noise (i_n) at 1 MHz. As a result of the transistor noise i_e, the D* at 1 MHz will be decreased by 18% relative to that at low frequencies, since

$$\frac{(1)^2}{(1)^2 + (1/2)^2} = 82\%$$

and $100\% - 82\% = 18\%$.

Appendix II
IMC-SCAN GEOMETRY

Consider the case of a scanner which is programmed in pitch, as shown in figure 21, so that consecutive scan lines are displaced a distance b along the ground track. Take the angular resolution to be $\beta = b/h$, where h is the scanner altitude. Thus, the scan lines just touch at the nadir. Notice that if the scanned angle is kept constant, the area scanned will show pincushion-like distortion perpendicular to the track as a result of the changing range from scanner to scanned line at the ground. Also notice that a variation of overlap both along and across the scan pattern will occur, resulting both from the changing range and also from the changing perspective (cosine effect) throughout the scan. Suppose that the variation in pitch of the scanner is from $+\alpha$ to $-\alpha$. If the lateral scan is limited to an angle of $\pm\phi$ the nominal width (u) of the scan pattern is $u = 2h \tan \phi$. Also, from the figure we see that while the patch of nominal dimensions $u \times u$ is scanned, the scanner must move a distance of $u + 2h \tan \alpha$. For a velocity of V this takes time $(u + 2h \tan \alpha)/V$. During this time the number of resolution elements scanned is:

$$\frac{u}{b} \times \frac{\phi}{\beta} \simeq \frac{u^2}{b^2}$$

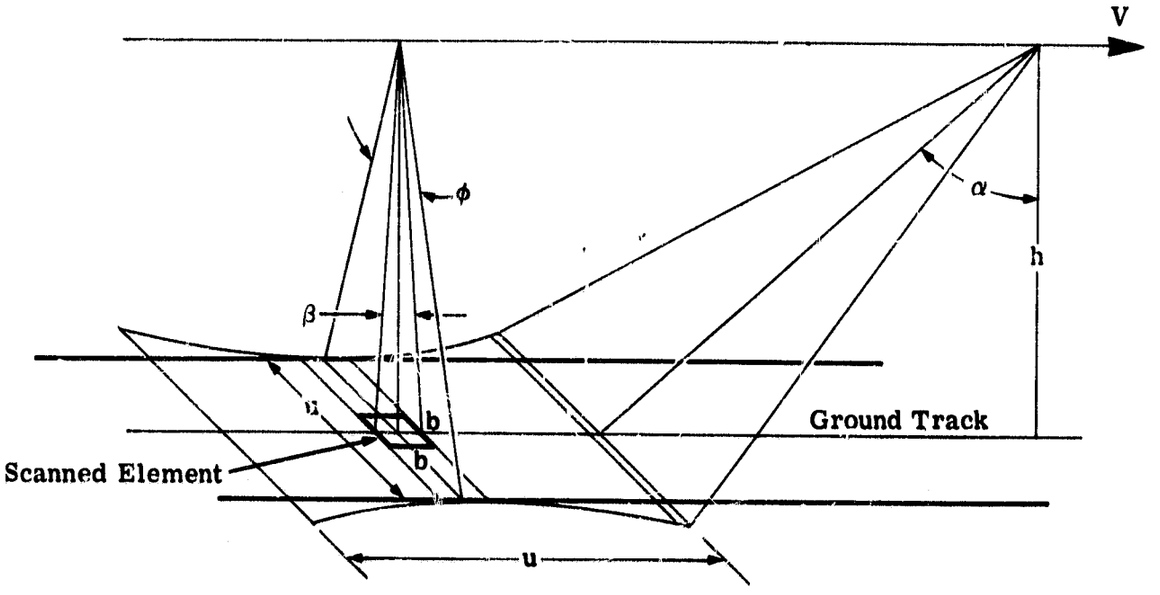

FIGURE 21. IMC-SCAN GEOMETRY

Thus, the rate at which elements are scanned, assuming perfect scanning efficiency, is:

$$\frac{u^2}{b^2} \cdot \frac{V}{u + 2h \tan \alpha}$$

Now assuming, as in section 3.4, that an analog bandwidth of 35 kHz is available for each spectral channel, the maximum value which this expression can take is 7.10^4 so that:

$$\frac{u^2 V}{b^2(u + 2h \tan \alpha)} = 7.10^4$$

A reasonable value for tan α is 0.05; for h, 250 nmi; and for V, 24,000 ft-sec^{-1}. Thus

$$\frac{u^2 2.4 \cdot 10^4}{b^2(u + 2 \cdot 250 \cdot 6000 \cdot 0.05)} = 7.10^4$$

or

$$\frac{u^2}{u + 1.5 \times 10^6} = 2.9b^2$$

Numerical solutions of this equation are given in table V. It will be seen that when b = 200 ft, u is about 70 nmi. Thus, from table I we see that a 20-nmi swath can be replaced by a 70-nmi square at this resolution.

TABLE V. RELATIONSHIP BETWEEN GROUND RESOLUTION AND SWATH WIDTH

u(ft)	u(nmi)	b(ft)
10^5	17	47
$2 \cdot 10^5$	33	90
$3 \cdot 10^5$	50	130
$4 \cdot 10^5$	67	170
$5 \cdot 10^5$	83	210
$7 \cdot 10^5$	117	280
10^6	167	370
$1.5 \cdot 10^6$	233	510

Appendix III
CONICAL-SCAN GEOMETRY

When a scan mirror is rotated about an axis close to its normal, the line of sight of a fixed telescope viewing the mirror, when deflected by the mirror, will follow a more or less conical pattern. To study this pattern more exactly, it is convenient to use the basic equations of spherical trigonometry as follows.

In figure 22, O is the center of a unit sphere; the other points lie on the surface of the unit sphere, and the lines shown joining these points are parts of great circles.

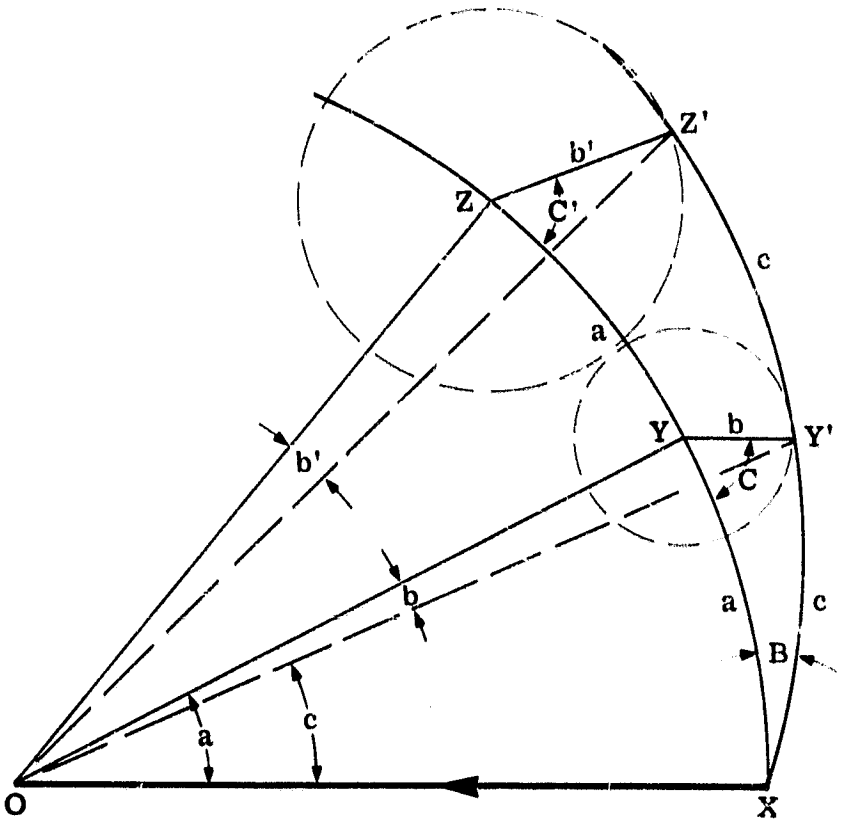

FIGURE 22. UNIT-SPHERE REPRESENTATION OF SCAN GEOMETRY

XO is the direction of the line of sight of the telescope, and OY is the direction of the axis of rotation of the scan mirror. If the angle between these two fixed directions is a, then the spherical distance XY is also a. Now if the normal to the mirror makes an angle b to OY, then this normal cuts the unit sphere at a point Y', such that Y' traces a small circle of radius b about Y as center.

Now as the angle of reflection equals the angle of incidence, the direction of the reflected ray must be OZ', such that Z'Y' = Y'X, and such that Z' lies on the great circle passing through

X and Y'. As Y' moves around Y, Z' must trace a closed path around Z, where Z lies on the great circle, through X and Y and such that ZY = YX.

For uniform rotation, the usual case, C increases uniformly with time and can be taken as an independent time variable. Thus, the problem is to find b' and C' as a function of C with, a and b as parameters. To do this, the following equations must be solved:

$$\cos c = \cos a \cos b + \sin a \sin b \cos C \tag{15}$$

$$\sin B = \sin b \frac{\sin C}{\sin c} \tag{16}$$

$$\cos b' = \cos 2c \cos 2a + \sin 2c \sin 2a \cos B \tag{17}$$

$$\sin C' = \sin 2c \frac{\sin B}{\sin b'} \tag{18}$$

There does not appear to be a useful closed solution to these equations, although numerical solution would be straightforward. However, the extent to which the locus departs from a circle can be seen from four simple cases:

(1) When C = ±O, i.e., when Y' lies on XYZ, then

$$\begin{aligned} b' &= ZZ' \\ &= ZX - Z'X \\ &= 2YX - 2Y'X \\ &= 2YY' = 2b \end{aligned}$$

(2) When $C \cong \pm\pi/2$ there are conditions at which Y'X = YX or c = a. We can then write (17) in the form

$$\cos b' = \cos^2 2a + \sin^2 2a \cos B$$

or considering b to be small

$$1 - \frac{b'^2}{2} \cong 1 - \sin^2 2a + \sin^2 2a \cos B$$

or

$$\frac{b'^2}{2} \cong \sin^2 2a(1 - \cos B)$$

Similarly we find

$$\frac{b^2}{2} \cong \sin^2 a(1 - \cos B)$$

so by dividing the last two equations we obtain

$$\frac{b'}{b} = \frac{\sin 2a}{\sin a} = 2 \cos a$$

or

$$b' = 2b \cos a$$

Thus, the diameter of the scan in this direction is less than that in the direction along XY by a fraction (1 - cos a). This departure is given in table VI for various values of a.

TABLE VI. DEPARTURE FROM CIRCLE

a	cos a	100 (1 - cos a)
10^o	0.985	1.5%
20^o	0.94	6%
30^o	0.865	13.5%
45^o	0.706	29.5%
60^o	0.5	50%

Appendix IV
ROTATING-CORNERS SCAN GEOMETRY

In thinking over mechanisms which might be used to carry out focal plane scanning over relatively small scan angles, we realized that a multicorner mirror drum as used in the Warner and Swasey Millisecond Wavelength Scanning Spectrometer [20] might provide an interesting solution.

Consider a corner formed by placing two plane mirrors at right angles, as shown in figure 23. If A is an object and O the apex of the corner, then it can be shown by simple geometry that rays from A reflected in both mirrors appear to diverge from a point B, which lies on AO extended, so that OB equals OA. Thus, if the apex of the corner is moved along the line OO', the image of A will move along a parallel line BB', such that AO'B' is a straight line and O'B' = O'A. Thus, if BB' lies in the focal plane of a collector, and if a small detector is placed at A, a scan is achieved when the corner is moved in an appropriate manner. (See fig. 24.)

If, following the Warner and Swasey system, we place a series of corners around the circumference of a drum, as indicated in figure 25, then as the drum is rotated, the image of the detector at A will move repeatedly along an arc BB' as each corner moves past the detector. Again, simple geometry shows that this arc is part of a circle, the radius of which is twice that on which the apexes of the corner mirrors lie.

An obvious implementation is to make the arc BB' lie on the spherical focal plane of a Schmitt-type collector. The drum is then seen to be rather large, obstructing the aperture.

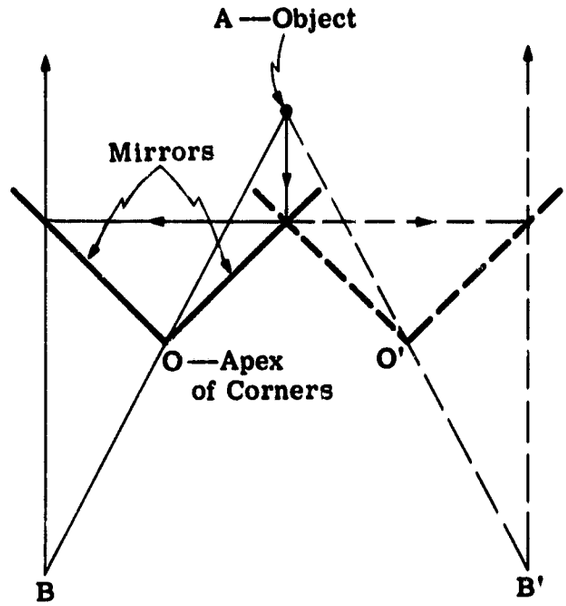

FIGURE 23. CORNER REFLECTOR-RAY DIAGRAM

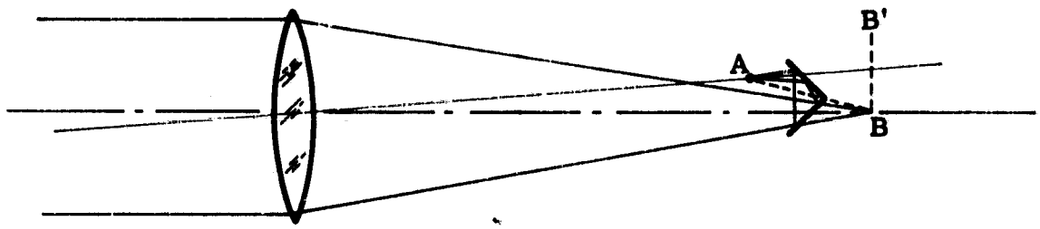

FIGURE 24. RAY DIAGRAM FOR CORNER REFLECTOR IN FRONT OF FOCAL PLANE

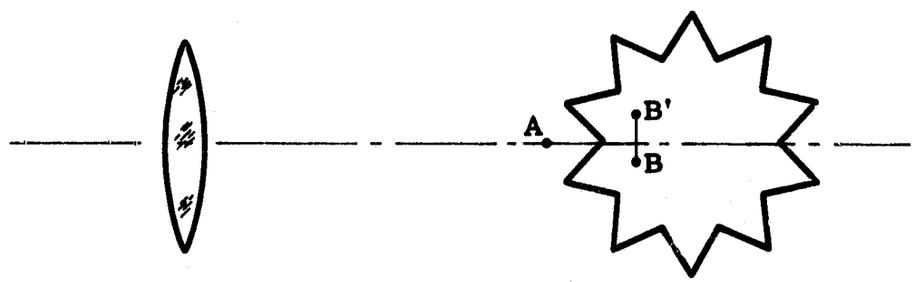

FIGURE 25. SCHEMATIC OF CORNER REFLECTOR DRUM

Thus, while this method appears practical in developing a system to cover a wide spectral range with high angular resolution, it seems that such a system would be somewhat cumbersome and would require considerable development.

Appendix V
HISTORY OF SPACECRAFT DATA LINKS FOR IMAGERY

Based upon information from references 21 through 30, figures 26 through 30 give block diagrams of the sensor and data links for several spacecraft systems, including the Lunar Orbiter, the Surveyor, the Ranger, and the Mariner IV. The figures also present the radiation-link parameters for each system except Lunar Orbiter, which was similar to the Surveyor wide-band system. (An explanation of equations relating these parameters is given in section 3.5.) Each system had only one image channel per data link, unlike the system we have been considering for a multispectral sensor. Lunar Orbiter had a film storage system and Mariner IV had a tape storage system, both of which could be used to slow down the data rate. Mariner used a storage register to reduce the data rate by reformating the data, entering it in the register during the 12% of the scan period when Mars was in the field of view and continually reading out. As a point of interest, one should note the varying number of resolution elements in each cycle of bandwidth used in the different spacecraft systems. As shown in table VII, the number varies from 1.42 to 2.0.

The Unified S-Band (USB) system [31] is a technique used by Jet Propulsion Laboratory during planetary shots to provide reliable tracking and communications. A single S-band carrier frequency is utilized in each direction for the transmission of tracking and communications data between the spacecraft and the ground. The transmitted carrier frequencies at the spacecraft are coherently controlled by the received carrier frequency, which allows measurements of the carrier doppler frequency by the ground station for determination of the radial velocity of the spacecraft. In addition, command data are modulated on the up carrier, and telemetry is modulated on the down carrier. Modulations and frequencies vary between programs, since USB is only a technique. Apollo USB, for example, is quite different from Mariner USB.

Appendix VI
LIMITATIONS ON SATELLITE TRANSMITTED POWER

On the basis of information drawn from reference 32, figure 31 was constructed to illustrate the maximum transmitter power-generation capability. A range of frequencies was pre-

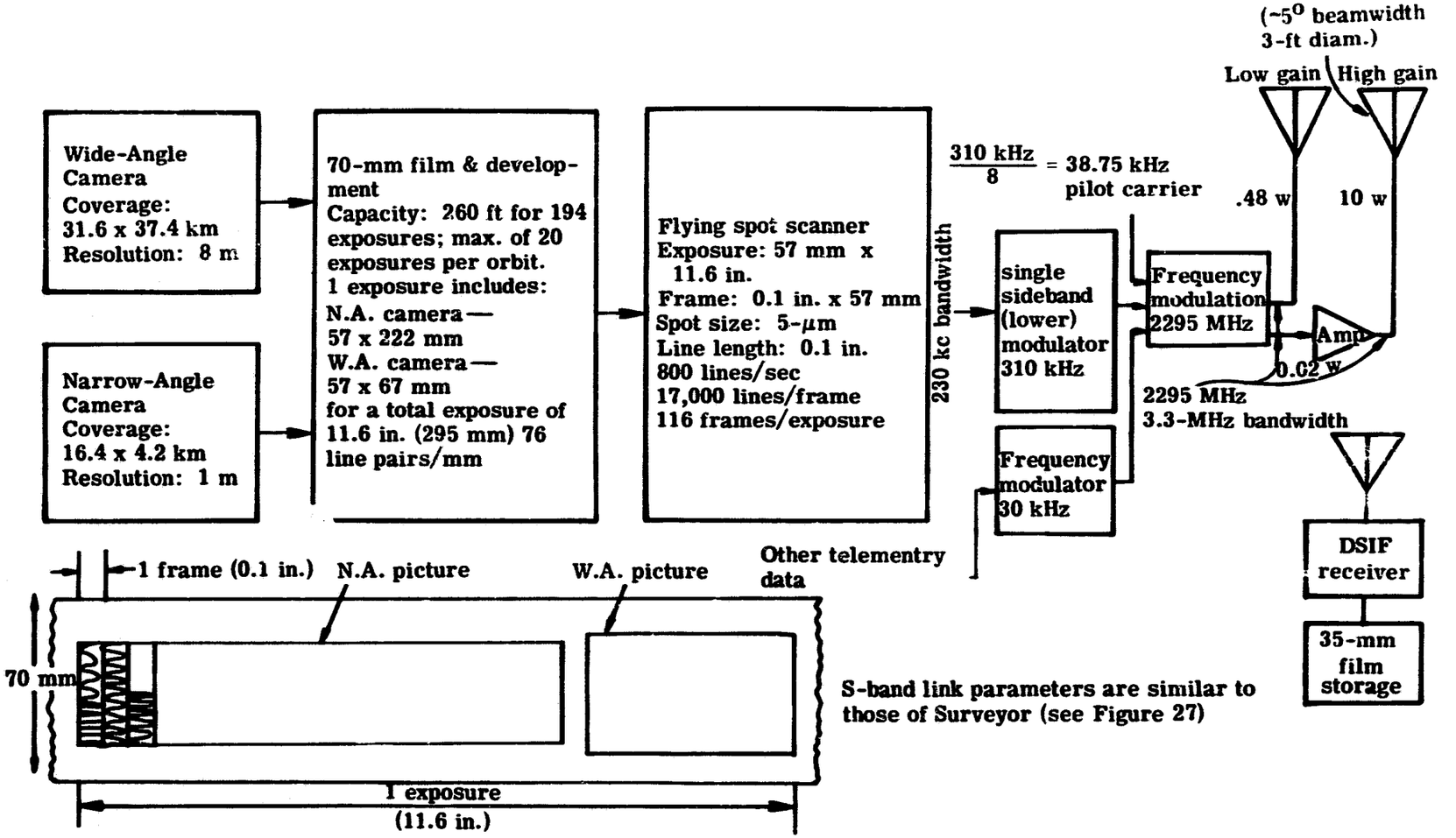

FIGURE 26. LUNAR ORBITER CAMERA AND DATA LINK

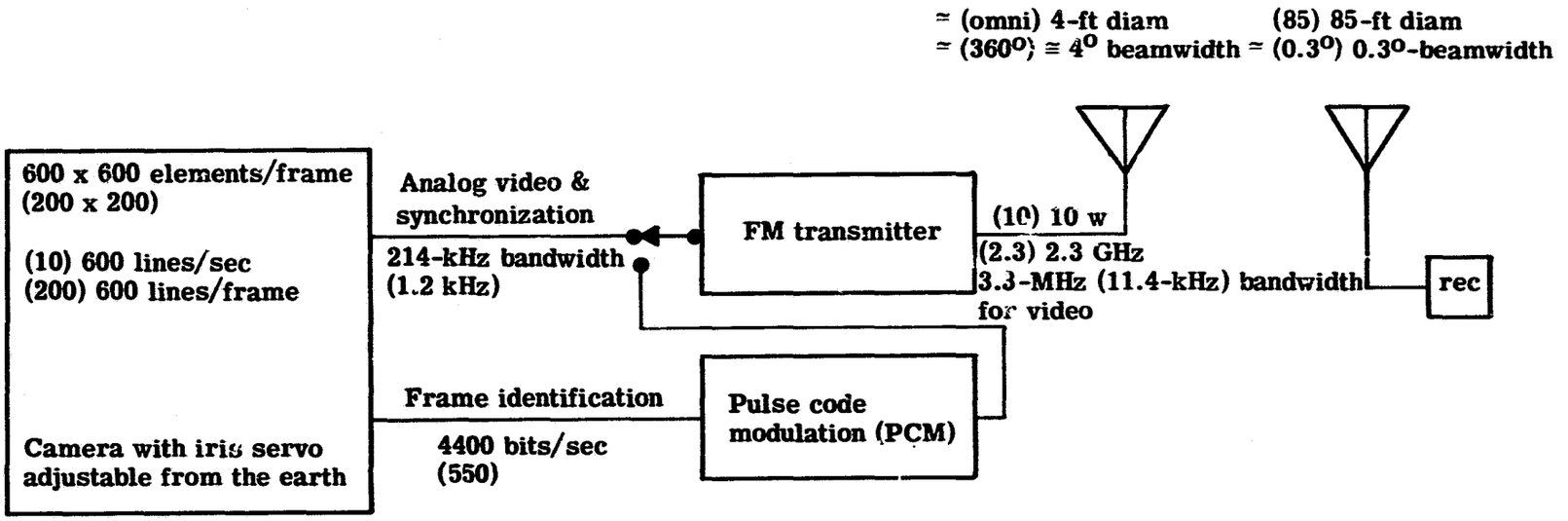

Combined telemetry & camera S/N > 63.
S/N = 255 worst for telemetry only
S/N = 398 nominal for telemetry only

$$S/N \equiv \frac{\text{video dynamic voltage range}}{\text{rms noise voltage in video bandwidth}}$$

Wideband-mode data not in parentheses
Narrowband-mode data in parentheses

S-band link (nominal conditions)	Wideband	Narrowband
10-w transmitter	+40. dbm	+40. dbm
Transmitter-antenna gain	+27. db	-2. db
Propagation loss	-211.9 db	-211.9 db
Atmos. atten.	0 db	0 db
Rec. antenna gain	+53. db	+53. db
Circuit loss	-2.5 db	-3.7 db
Rec. power	-94.4 dbm	-124.6 dbm
Rec. bandwidth (above Hz)	+65.2 db	40.6 db
Rec. power/Hz	-159.6 dbm/Hz	-165.2 dbm/Hz
Rec. noise/Hz	-176.3 dbm/Hz	-176.5 dbm/Hz
Rec. S/N	16.7 db	11.3 db

FIGURE 27. SURVEYOR SURVEY CAMERA AND DATA LINK

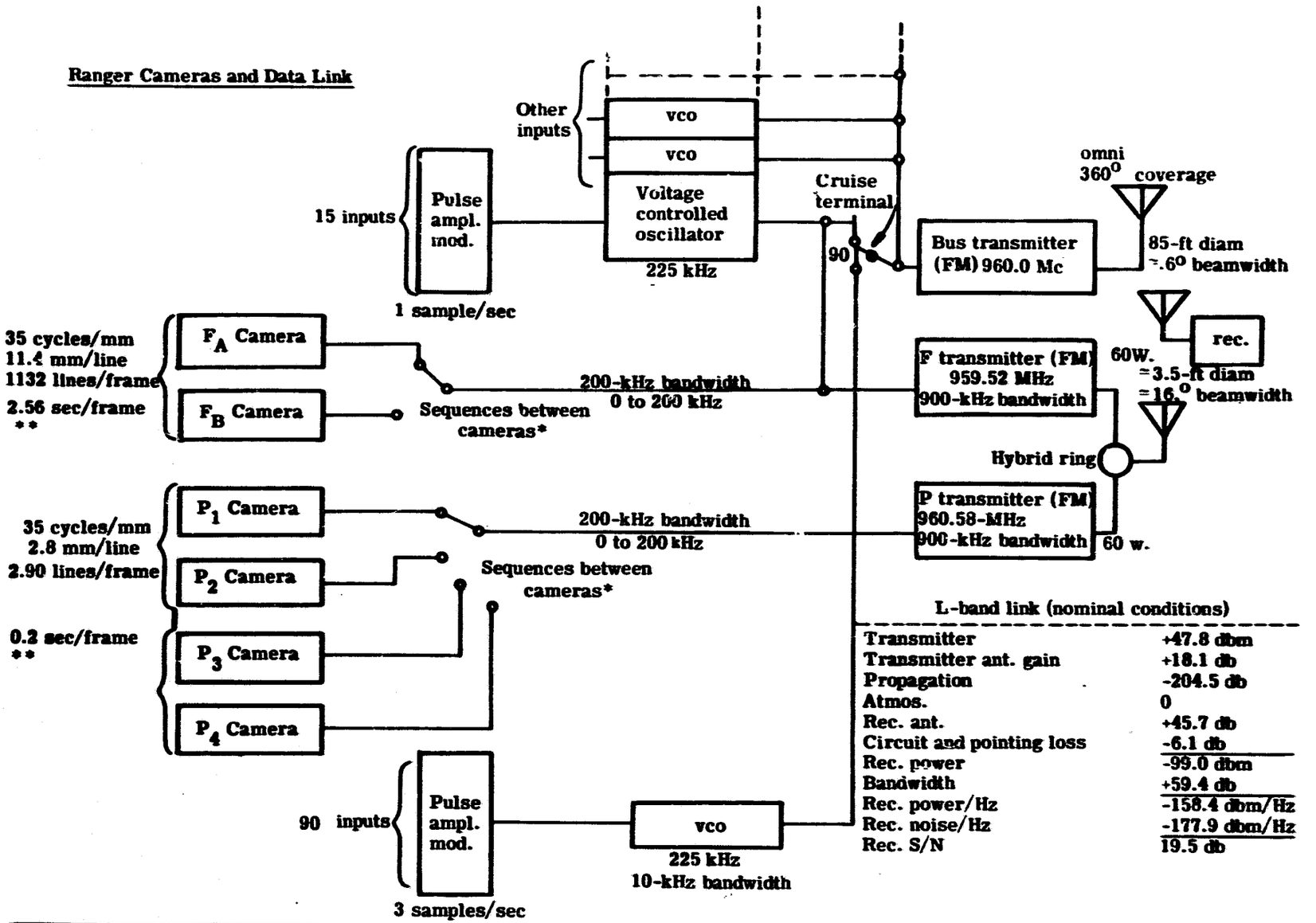

*When a camera Vidicon is not being read, it is either being exposed or erased.
**The system gain and level was preset in the system design; therefore it couldn't be changed during the flight.

FIGURE 28. RANGER CAMERAS AND DATA LINK

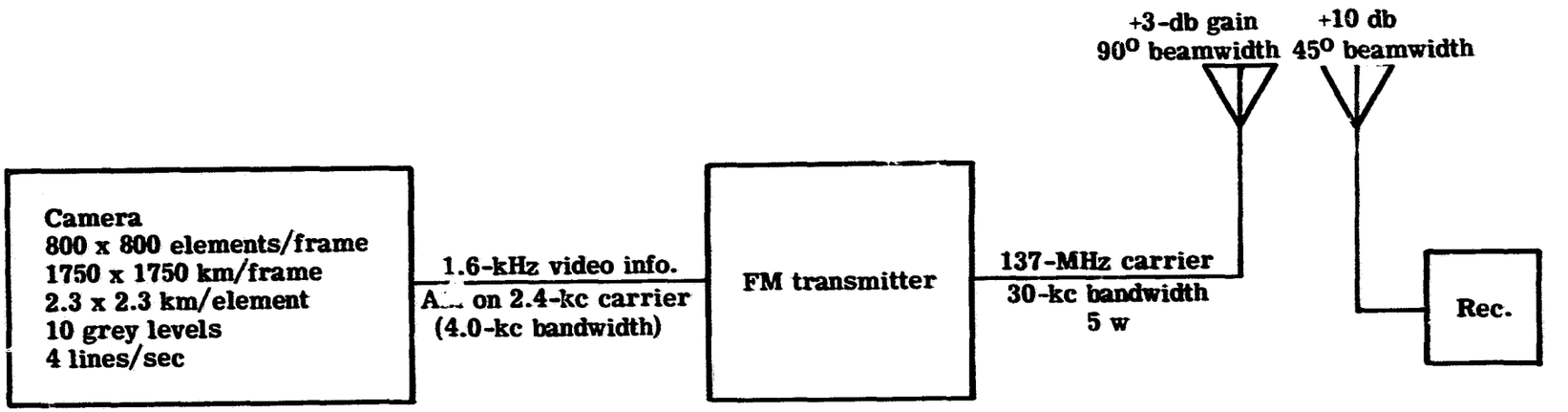

137 MHz link	
Transmitter	+37 dbm
Transmitter ant. gain	+3 db
Propagation	-146.2 db
Atmos.	0
Rec. ant.	+10 db
Circuit and pointing loss	-5.8 db
Rec. power	-102 dbm
Bandwidth	+44.8 db/Hz
Rec. power/Hz	-146.8 dbm/Hz
Rec. noise/Hz	-166.9 dbm/Hz
Rec. S/N	20.1 db

FIGURE 29. AUTOMATIC PICTURE TRANSMISSION CAMERA AND DATA LINK. 900-km polar earth orbit. AM-FM.

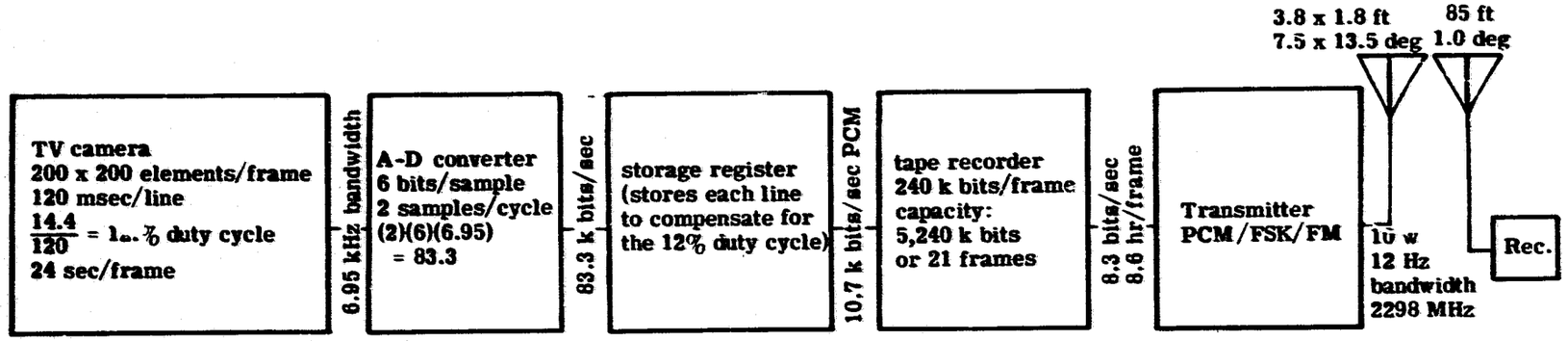

S-band link (nominal conditions)	
Transmitter	+40.0 dbm
Transmitter ant. gain	+23.2 db
Propagation	-266.5 db
Atmos.	0
Rec. ant.	+53.0 db
Circuit and pointing loss	-6.3 db
Rec. power	-156.6 dbm
Bandwidth	+10.8 db
Rec. power/Hz	-167.4 dbm/Hz
Rec. noise/Hz	-181.2 dbm/Hz
Rec. S/N	13.8 db

FIGURE 30. MARINER IV CAMERA AND DATA LINK

TABLE VII. SPACECRAFT DATA LINKS

	No. of Resolution Elements/sec. Hz of Video Bandwidths	Radiation Bandwidth Video Bandwidth	No. of Grey Levels in Total System
Lunar Orbiter	1.77	14.3	15
Surveyor	1.68	15.4	63
Ranger	1.76 (F cameras) 1.42 (P cameras)	4.5	5-75*
APT	2.00	18.8	10
Mariner	2.00	digital	64

*Depends on light level (for cameras only)

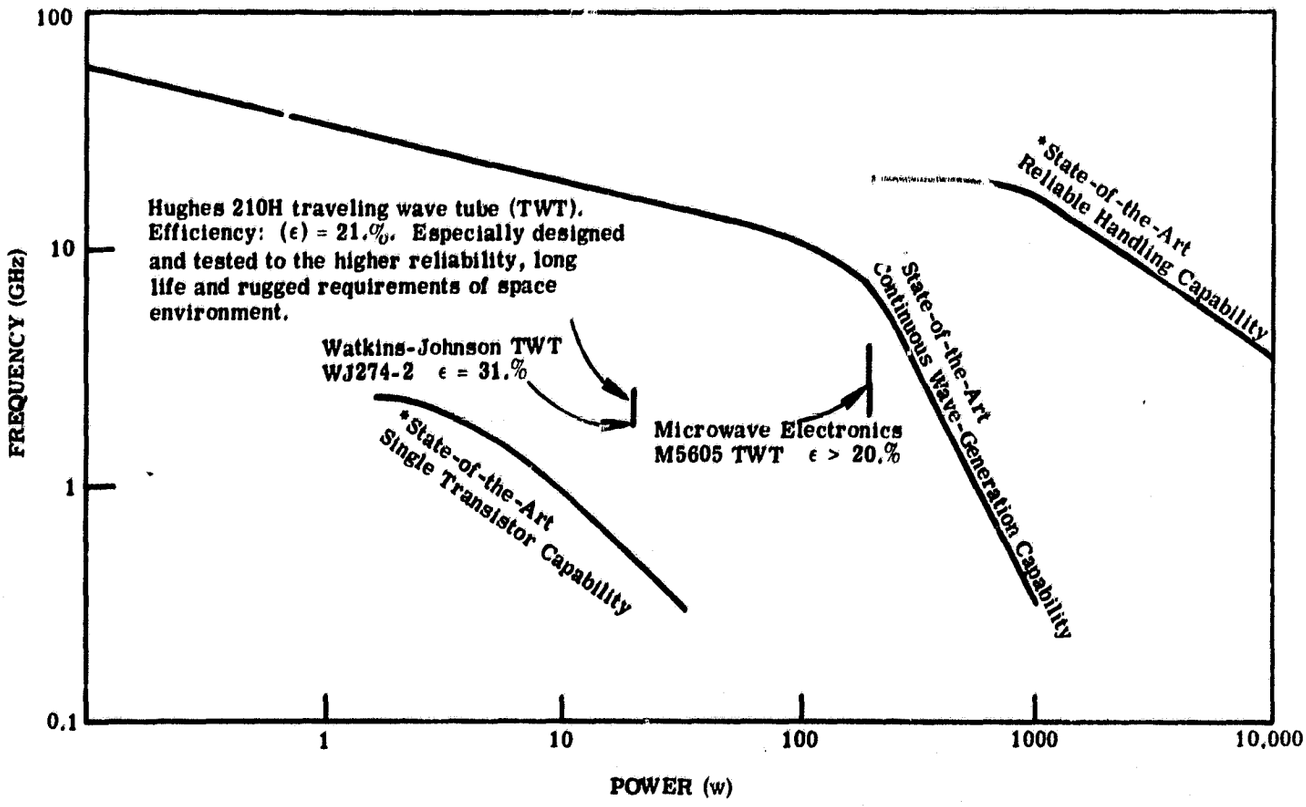

FIGURE 31. TRANSMITTER POWER CAPABILITY

sented because it may be necessary to operate at a higher frequency than S-band (2.29 to 2.30 GHz is allocated for space telemetry) in order to minimize other telemetry interference, to reduce galactic noise, and to obtain larger bandwidths. The three traveling wave tubes (TWT) illustrated have either high efficiency, high reliability, or high power. For the immediate future,

20 w should probably be considered the upper limit (unless a large penalty results), even though higher power TWT can be constructed.

Because of limited efficiency, only 50% of the power from a power source can be supplied to a TWT, while a good TWT has an efficiency of about 20%, which means that the power source must supply ten times the power that can be transmitted. Although power sources in the megawatt range are feasible for space applications [15], because of weight and other considerations, only much more modest powers will be available in the near future. The source power available for a particular mission is, then, likely to be a more stringent limitation than availability of transmitter equipment.

Appendix VII
NASA GROUND-SUPPORT INSTRUMENTATION NETWORK

General

The NASA ground-support instrumentation presently consists of four major networks:

(1) The Manned Spaceflight Network (MSFN)
(2) The Space Tracking and Data Acquisition Network (STADAN)
(3) The Deep-Space Instrumentation Facility (DSIF)
(4) The Smithsonian Astrophysical Observatory (SAO)

Only the first three are of interest to our present study, since the fourth (SAO) is an optical tracking facility using Baker-Nunn telescopic cameras. In fact, only the first two are of prime concern in an earth-orbital situation, since DSIF is designed to support lunar and planetary probes wherein the tracking rate is less important than precision and sensitivity. Consequently, antenna design is governed by different considerations, and performance in an earth-orbital tracking application is considerably reduced. Thus, the following discussion primarily concerns MSFN and STADAN, with a few aspects of DSIF included for comparison only. (A useful general description of the STADAN is given in reference 33.)

Antenna Mounts

There are three basic antenna mounts, differing primarily in the orientation of the lower of two mutually perpendicular axes. These are: (1) azimuth-elevation (Az-El), (2) Right Ascension (or hour angle)-Declination (RA-Dec, HA-Dec, or Polar), and (3) X-Y, (see fig. 32).

The Az-El mount (fig. 32a) has its lower axis vertical and its upper axis horizontal. Both axes remain in their respective planes throughout the antenna's tracking range. This arrange-

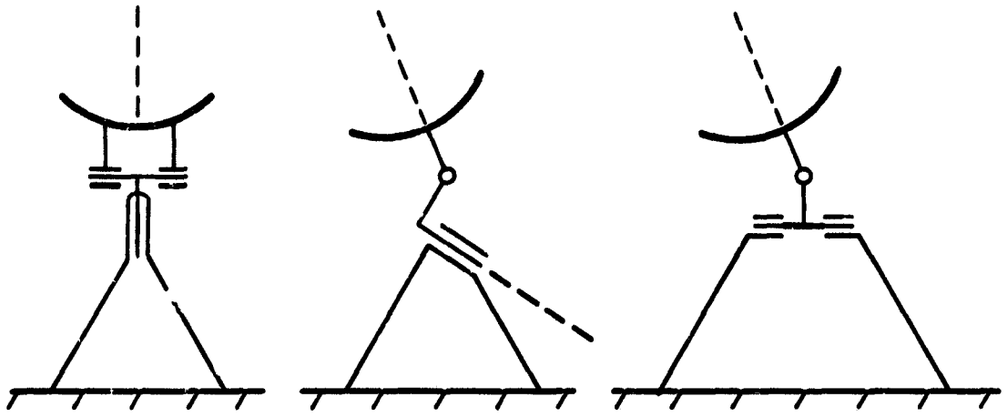

FIGURE 32. ANTENNAE MOUNTS

ment provides compactness and rigidity, reduces counter balancing and maintenance problems,* and is the most popular mount when tracking through zenith is not essential. However, very fast azimuth rates are necessary to avoid a critical hole in tracking capability near zenith. Such holes (called keyholes) are common to all antenna mounts and are localized to cones around the ends of the lower axis. Because of the orientation of this axis in the Az-El configuration, such mounts are limited to horizon-acquisition and shipboard-tracking applications. In the latter application, the mount's compactness, lighter weight, and lower moment of inertia about the lower axis outweigh its disadvantages near zenith (especially since a ship's location can normally be selected to avoid a direct overhead tracking requirement).

The Polar mount (fig. 32b) differs from Az-El only in having its lower axis tipped parallel to the earth's rotational axis. This type of mount is ideally suited to astronomical applications, since celestial sources can be tracked by rotation about a single axis. In this case, high tracking rates are obviously of little importance, and a relatively large hole (below an hour-angle arc through the earth's rotational pole) is of little consequence. However, for earth-orbital satellite tracking, a large area of the sky is inaccessible. Further, since both axes must rotate through angles greater than 90°, stress reversals occur throughout the antenna structure. Counter-balancing about both axes relieves this problem somewhat but at the expense of the Az-El mount's compactness.

*Since rotation about the upper (horizontal) axis is limited to somewhat less than 90°, only those parts below the azimuth axis undergo stress reversal.

The final mount, X-Y (fig. 32c), was designed specifically for earth-orbital satellite tracking to alleviate the zenith keyhole by moving the lower axis into the local tangent plane. The upper axis rotates about the lower axis such that it is horizontal (and normal to the lower axis) when the antenna is pointed at local zenith. Although such an arrangement allows complete freedom of zenith tracking with no excessive rotational rates (as in Az-El), there are several disadvantages. In order to obtain complete sky coverage (or to minimize the keyhole at each end of the lower axis), the two axes must be rather widely separated. This requirement necessitates careful counter-balancing for both axes, increases overall size, weight, and cost, reduces compactness and rigidity, and increases moments of inertia. Nevertheless, NASA has established that a zenith-tracking capability is required for all land stations and except for shipboard systems, the X-Y mount is used exclusively.

This discussion need not eliminate the suggestion that the 85-ft dish at Peach Mountain (RA-Dec) be considered, although at our latitude a large (but not necessarily prohibitive) region of the northern sky is lost. Use of the Peach Mountain dish appears superfluous, however, even though physically accessible to us, since the United States is already adequately covered by STADAN.

Antennas Presently Available

Disregarding mobile vans as well as aircraft and shipboard facilities, which seen to come and go among various networks as the need arises, we have some 24 to 30 receiving stations spread around the world in MSFN and STADAN.* These include at least six different data-acquisition antennae (present at the different sites either singly or in a variety of combinations); 9 and 16 Yagi arrays, primarily for 136-140-Mc operation; and 14-, 30-, 40- and 85-ft, solid-surface parabolas, designed for use through X-band. In addition, DSIF includes 85-ft (and one 210-ft) parabolas, designed for lower tracking rates but useable for orbital altitudes above 400 nmi (see fig. 33).

STADAN has two 14-ft, seven 40-ft, and five 85-ft parabolas. MSFN has ten 30-ft and three 85-ft units, although some are counted in both networks. However, there are at least two 14-ft, ten 30-ft, seven 40-ft, and five 85-ft X-Y mounts in existence in both networks. Sites are distributed as shown in table VIII.

In general, STADAN concentrates upon tracking and data acquisition from unmanned satellites, while MSFN handles all manned vehicles. However, in some cases they share a common site and occasionally common equipment as well. Both networks use X-Y mounts but orient

*The actual number varies, depending upon just which stations are or are not included in a given network for a given mission.

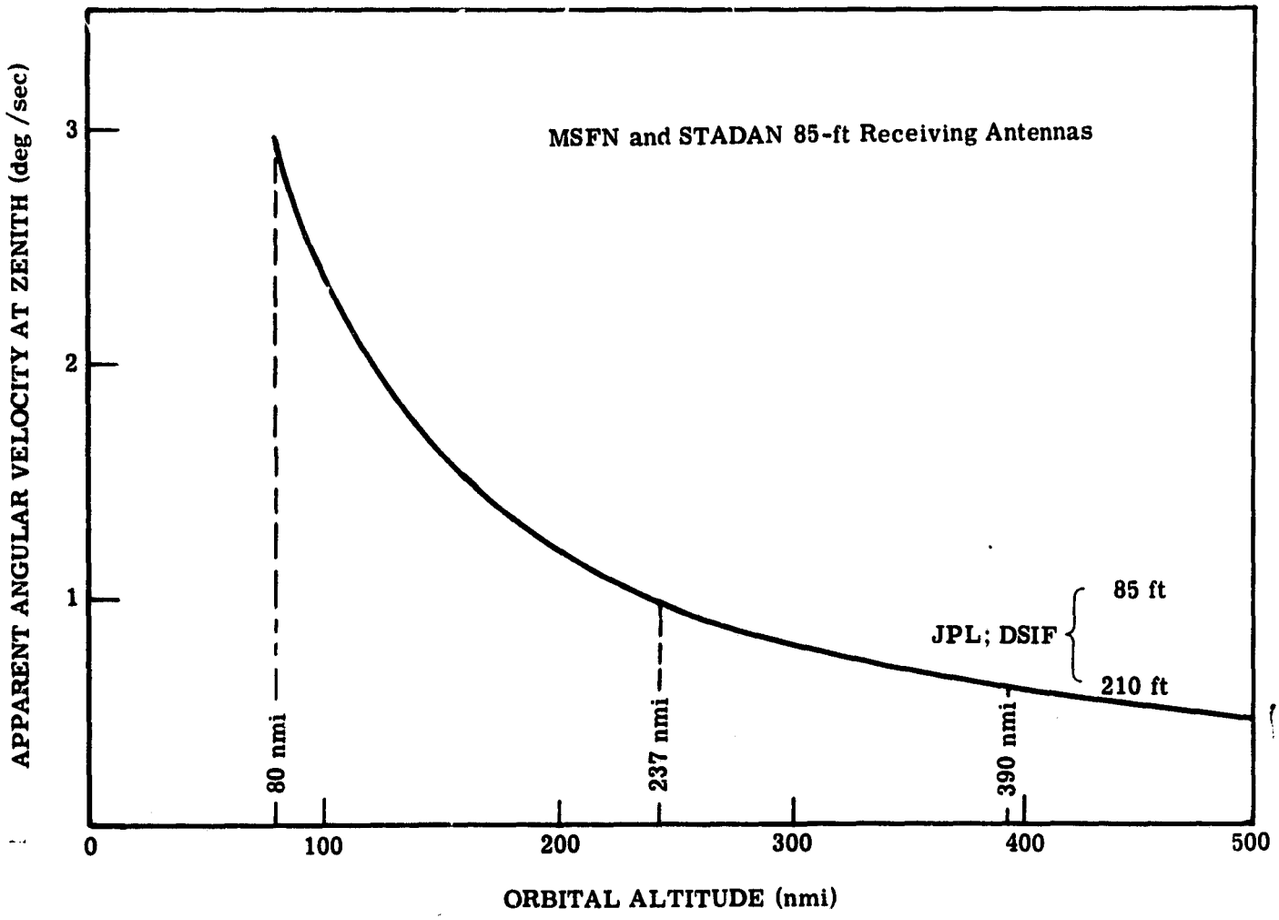

FIGURE 33. MAXIMUM APPARENT ANGULAR VELOCITY (RATE OF CHANGE OF ELEVATION ANGLE AT ZENITH) FOR EARTH SATELLITES IN CIRCULAR ORBIT AND MINIMUM ALTITUDE-TRACKING CAPABILITY FOR VARIOUS NETWORKS AND ANTENNAE

their lower axes in different directions. STADAN stations are distributed around the globe in a generally north-south direction and consequently orient the lower axes of their antennae in this direction.* MSFN stations, more equatorially distributed, have their lower axes oriented east-west.† In this way, each station's keyholes can be filled by an adjacent station, resulting in complete sky coverage.

Antennae Tracking Capability

General tracking specifications are given in table IX for the larger antennae (applicable to both networks). If we refer to figure 34 and assume a circular orbit:

*85-ft antennae. Some smaller dishes are oriented normal to these directions.

†Full accuracy to 20 mph; tolerance doubled 20-30 mph and quadrupled 30-45 mph.

TABLE VIII. GLOBAL DISTRIBUTION OF MSFN AND STADAN SITES

MSFN	STADAN
Antigua	Alaska
Ascension	Australia
Australia	California
Bahamas	Chile
Bermuda	Ecuador
Canary	England
Canberra	Florida
Goldstone	Hawaii
Guam	Malagasy Republic
Guaymas	Newfoundland
Hawaii	North Carolina
Madrid	Peru
Mila	South Africa
Texas	

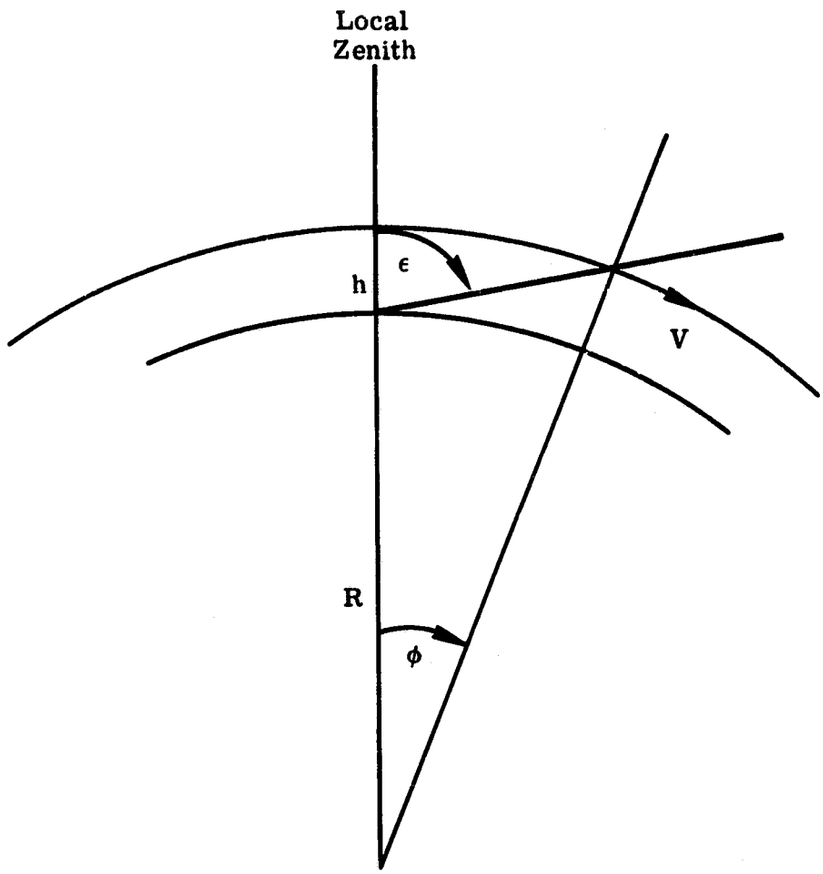

FIGURE 34. SKY COVERAGE DIAGRAM

TABLE IX. GENERAL SYSTEM SPECIFICATIONS

	MSFN and STADAN		DSIF	
	30 & 40 ft	85 ft	85 ft	210 ft
Track Velocity (^{o}/sec)	4	3	1	0.6
Track Accel. (^{o}/sec^2)	5	5		
Wind: Full Accuracy (mph)	20	20		
Reduced Accuracy (mph)*	45	45		
Sky Coverage (deg above horizon)	2	2		
Keyhole Cone	20	20		
Accuracy (min)				
Pointing	±0.6	±0.6		
Tracking	1.5 max.	1.5 max.		

*Full accuracy to 20 mph; tolerance doubled 20-30 mph and quadrupled 30-45 mph.

$$\frac{\partial \epsilon}{\partial t} = \frac{R + h}{h} \frac{\partial \phi}{\partial t} \quad \text{(at zenith)}$$

where t = time

h = orbital altitude

R = radius of earth

ϕ = angle subtended at the center of the earth between the satellite and the antenna

ϵ = zenith angle of the satellite measured from the antenna

This equation results from the following considerations. Only zenith is considered, since $\frac{\partial \epsilon}{\partial t}$ is maximum at zenith. If $\frac{\partial \epsilon}{\partial t}$ is less than 3 deg/sec (maximum rate of 85-ft dish), the satellite can be tracked at any other elevation angle. It is straightforward to show that for a circular orbit:

$$\epsilon = \cot^{-1}\left[\cot \phi - \frac{R}{(R + h) \sin \phi}\right]$$

$$\frac{\partial \epsilon}{\partial \phi} = -\sin^2 \epsilon \left[\frac{R \cos \phi - (R + h)}{(R + h) \sin^2 \phi}\right]$$

and that the latter varies between $[(R + h)/h]_{\text{zenith}}$ and $(1.0)_{\text{horizon}}$. Thus, an antenna must be capable of a velocity $[(R + h)/h]\, d\phi/dt$ deg/sec for zenith (therefore complete) tracking of a satellite at altitude h.

Thus, the maximum apparent angular velocity for various altitudes can be calculated and compared to known antenna tracking capabilities. These are plotted (for circular orbits) in figure 33, where, for example, it is seen that Jet Propulsion Laboratory's DSIF, 210-ft antenna could track through zenith an earth-orbital satellite in a circular orbit above 400 nmi; the DSIF 85-ft antenna above 240 nmi; and the MSFN or STADAN 85-ft antenna above any practical earth-orbital altitude.

While the STADAN and MSFN systems do not provide complete world-wide acquisition of satellite transmissions, the coverage of much of the world's land mass and several ocean areas is good. The most important areas not presently covered are the Soviet Union and, unfortunately, the broad strip of land and sea running from the Sahara eastward across northern and central Africa, the Near East, and southern Asia into Southeast Asia.

Summary

It appears that MSFN and STADAN presently provide fairly adequate coverage and tracking capability for any earth satellite, since 80 nmi is considered a practical lower limit because of atmospheric heating and mission lifetime. Also, everyone we talked to generally agreed that 85-ft antennae are the largest one should consider for the tracking of earth-orbital satellites. either now or in the foreseeable future, because of the cost of larger structures. All agreed that any further gains would have to come at the satellite end, if absolutely necessary to a given mission, either through transmitter power or satellite antennae.

Further, since DSIF antennae do allow tracking of the higher-altitude satellites, it is at least conceivable that they could be considered. However, no widespread DSIF network (such as MSFN or STADAN) is ever foreseen, and any earth-orbital mission would be superceded by deep-space probes.

It is generally agreed that even Jet Propulsion Laboratory's 210-ft dish could have been designed for a higher tracking-rate capability but at astronomical cost (at least 10-20 million dollars). Some sources felt that a 100-ft, 3-deg/sec dish was feasible but not one of 150-ft. Generally, it appears that one should consider the present 85-ft antenna as maximum size. More antennae may eventually become available, but not larger ones.

REFERENCES

1. B. Leo, "Heat Powered Vuilleumier Refrigerator for Cooling Infrared Detectors," Proc. IRIS, Vol. 14, No. 1. (in publication)
2. D. E. Bode, P. R. Bratt, and R. L. Nielsen, "Characteristics of Cadmium-Doped Germanium Compared to Mercury- and Copper-Doped Germanium under Low Background Conditions (U)," Proc. IRIS, Vol. 13, No. 1, April 1969, pp. 199-207 (CONFIDENTIAL).
3. R. O. Wageneck and R. L. Williams, "Photoconductivity of Extrinsic Doped Germanium at Reduced Backgrounds (U)," Proc. IRIS, Vol. 13, No. 2 (CONFIDENTIAL). (in publication)
4. D. E. Bode and H. A. Graham, "A Comparison of the Performance of Copper-Doped Germanium and Mercury-Doped Germanium Detectors," Proc. IRIS, Vol. 8, No. 3, August 1963, pp. 105-116.
5. D. E. Bode, P. R. Bratt, H. A. Graham, and R. L. Nielsen, "Characteristics of Mercury-Doped Germanium Detectors Under Reduced Background Conditions," Proc. IRIS, Vol. 10, No. 3, January 1966, pp. 81-88.
6. D. E. Bode, H. A. Graham, and R. L. Nielsen, "The Effect of Background Radiation on Copper- and Mercury-Doped Germanium (U)," Proc. IRIS, Vol. 9, No. 3, September 1964, pp. 107-110 (CONFIDENTIAL).
7. H. Pullan, "A Cooled Detector-Preamplifier System for Detection (U)," Proc. IRIS, Vol. 10, No. 3, September 1964, pp. 111-115 (CONFIDENTIAL).
8. W. L. Brown and C. T. Yang, "Mechanics of Rotating Plates and Prisms," Report No. 2900-251-T, Willow Run Laboratories, Institute of Science and Technology, The University of Michigan, Ann Arbor, February 1961.
9. W. L. Brown, M. E. Bair, and R. T. Nalepka, "Effect of Surface Deformations in Rotating Oblique Scanning Mirrors on Image Quality in Flying Spot Scanners," Report No. 2900-469-T, Willow Run Laboratories, Institute of Science and Technology, The University of Michigan, Ann Arbor, April 1964.
10. "A Study of High V/H Infrared Line Scanning Systems (U)," Technical Documentary Report ASD-TDR-63-390, Wright Air Development Center, Air Research and Development Command, USAF, Wright-Patterson Air Force Base, Ohio, March 1963, Prepared under Contract Number AF33(657)-8870 by HRB-Singer, Inc., State College, Pa. (CONFIDENTIAL).
11. S. Timoshenko and S. Woinowsky-Krieger, "Theory of Plates and Shells," 2nd Edition, McGraw-Hill, New York, N. Y., 1959.
12. Private Communications: I. L. Goldberg, NASA/Goddard Space Flight Center, November 1968.
13. Private Communication: J. C. Moody, NASA/Goddard Space Flight Center, November 1968.
14. J. Braithwaite, "Dispersive Multispectral Scanning," Report No. 7610-5-F, Willow Run Laboratories, Institute of Science and Technology, The University of Michigan, Ann Arbor, September 1966.
15. E. L. Gruenberg, Handbook of Telemetry and Remote Control, McGraw-Hill, New York, N. Y., 1967.
16. L. H. Bedford, "Television by Satellite," Radio Electronic Eng., November 1968, pp. 273-283.

17. W. F. Link and C. D. Eatough, "Experimental Optimization and Evaluation ... Telemetry Systems," IRE Trans. on Space Electronics and Telemetry, September 1962, pp. 239-246.

18. D. G. Childers, "Evaluation of Techniques for PCM Range Telemetry," Proc. Nat'l. Telemetering Conference, Santa Monica, Calif., May 22-24, 1960, pp. 27-289.

19. W. P. McGarry, "A Multiplexed FM Data System with Identical Channel Characteristics," Internal Memo, Data Control Systems, Danbury, Conn.

20. Warner and Swasey Co., Control Instrument Division, Flushing, N. Y., 11354, Brochure No. 1164-5M-TV-A.

21. L. J. Kosofsky and G. C. Broome, "Lunar Orbiter: A Photographic Satellite," J. Soc. Motion Picture Television Engrs., Vol. 74, September 1965.

22. A. Jensen et al., "Lunar Orbiter Readout," J. Soc. Motion Picture Television Engrs., Vol. 76, August 1967.

23. R. A. Grammer et al , "Ground Reconstruction of Lunar Orbiter Photography," J. Soc. Motion Picture Television Engrs., Vol. 76, August 1967.

24. R. J. Rechter, "Signal Processing and Transmission for the Surveyor Television System," J. Soc. Motion Picture Television Engrs., April 1968, p. 341.

25. D. H. Kindt and J. R. Staniszewski, "The Design of the Ranger Television System to Obtain High Resolution Photographs of the Lunar Surface," Technical Report No. 32-717, Jet Propulsion Laboratory, Pasadena, 1965.

26. R. A. Stampfl and W. G. Stroud, "Automatic Picture Transmission TV Camera System for Meteorological Satellites," J. Soc. Motion Picture Television Engrs., February 1964, p. 130.

27. J. C. Moody and O. Weinstein, "Night and Day, Nimbus 2 Transmits Its Cloud Pictures," Electronics, 22 August 1966, p. 121.

28. J. D. Allen, "A Mars Spacecraft Photographic System," J. Soc. Motion Picture Television Engrs., June 1965, pp. 497-500.

29. Mariner Mars 1964, Project Report: Television Experiment; Part I—Investigators' Report, Jet Propulsion Laboratory Technical Report No. 32-884, 1967.

30. R. P. Mathison, Mariner Mars 1964, Telemetry and Command System, Jet Propulsion Laboratory Technical Report No. 32-684, 1965.

31. Proceedings of the Apollo United S-Band Technical Conference, NASA SP-87, July 1965.

32. F. A. Brand and V. Gelnovatch, Microwave Engineers' Handbook and Buyers Guide, Horizon House, Dedham, Mass., 1968.

33. "Space Tracking and Data Acquisition Network Manual," a report from Goddard Space Flight Center, July 1967.